The origin of intestinal cancer in the context of inflammation

Mathijs P. Verhagen[1], Rosalie Joosten[1], Mark Schmitt[1,2], Niko Välimäki[3,4], Andrea Sacchetti[1], Kristiina Rajamäki[3,4], Jiahn Choi[5], Paola Procopio[2], Sara Silva[2], Berdine van der Steen[6], Thierry P.P. van den Bosch[1], Danielle Seinstra[1], Michail Doukas[1], Leonard H. Augenlicht[5], Lauri A. Aaltonen[3,7], and Riccardo Fodde[1]*

[1]Department of Pathology, Erasmus University Medical Center, Rotterdam, The Netherlands.

[2]Institute of Pharmacology, University of Marburg, Germany.

[3]Department of Medical and Clinical Genetics, University of Helsinki, Helsinki, Finland.

[4]Applied Tumor Genomics Research Program, Research Programs Unit, University of Helsinki, Helsinki, Finland.

[5]Department of Cell Biology, Albert Einstein College of Medicine, New York, U.S.A.

[6]Department of Otorhinolaryngology and Head & Neck Surgery, Erasmus University Medical Center, Rotterdam, The Netherlands.

[7]iCAN Digital Precision Cancer Medicine Flagship, University of Helsinki, Helsinki, Finland.

*to whom correspondence should be addressed at:

Erasmus MC, Department of Pathology, PO Box 2040, 3000 CA Rotterdam, The Netherlands

E-mail: r.fodde@erasmusmc.nl Tel: +31 10 7043896

Abstract

Paneth cells (PCs), responsible for the secretion of antimicrobial peptides in the small intestine and for niche support to *Lgr5*$^{+}$ crypt-base columnar stem cells (CBCs), have been shown to respond to inflammation by dedifferentiating into stem-like cells in order to sustain the regenerative response[1,2]. As such, PCs may represent the cells-of-origin of intestinal cancer in the context of inflammation.

To test this hypothesis, we targeted *Apc*, *Kras*, and *Tp53* mutations in Paneth cells by Cre-Lox technology in the mouse and modelled inflammation by dextran sodium sulfate (DSS) administration. PC-specific loss of *Apc* resulted in multiple small intestinal tumors, whereas *Kras* or *Tp53* mutations did not. Compound *Apc* and *Kras* mutations in PCs resulted in a striking increase in tumor multiplicity even in the absence of the inflammatory insult. By combining scRNAseq with lineage tracing to capture the conversion of PCs into *bona fide* tumor cells, we show that they progress through a "revival stem cell" (RSC) state characterized by high *Clusterin* (*Clu*) expression and *Yap1* signaling, reminiscent of what has previously been observed upon irradiation[3]. Accordingly, comparison of CBC- with PC-derived murine intestinal tumors revealed differences related to Wnt signaling and inflammatory pathways which match the dichotomy of CBCs and injury-induced RSCs[4] between human sporadic colon cancers and those arising in the context of inflammatory bowel diseases. Of note, a striking ~25% of sporadic colon cancers show expression profiles similar to those of PC-initiated mouse tumors and of patients with an IBD history. The latter can be explained by the low-grade, subclinical inflammation induced by western-style dietary habits, the major colon cancer risk factor, likely to underlie the de-differentiation of secretory lineages of the colon and their acquisition of stem-like and tumor-initiating features. To validate these observations, we applied novel computational methods[5-7] to predict the cell of origin of tumors by matching their genome-wide mutation spectrum with the epigenetic landscapes of colonic cell lineages. While the majority of sporadic colon cancers are predicted to originate from stem cells, in patients with an IBD history, the predominant cell of origin switches to secretory lineages such as goblet cells.

Taken together, our results show that, in the context of inflammation, intestinal cancer arises through the dedifferentiation of committed secretory lineages and the activation of the revival stem cell state. The chronic nature of the inflammatory insult caused by western-style dietary habits is likely to underlie similar mechanisms in a significant proportion of sporadic colon cancers and warrants a novel stratification of the cases for improved clinical management.

Paneth cells as the origin of intestinal tumors in the context of inflammation and loss of *Apc*.

The origin of the vast majority of cancers is thought to reside in stem- or progenitor-like cells which satisfy the needs for active proliferation, self-renewal, and differentiation capacity. This was demonstrated in the intestine where loss-of-function mutations in the *Apc* tumor suppressor gene successfully initiate adenoma formation only when they occur in *Lgr5*$^{+}$ CBCs. When the same *Apc* mutation is introduced in more committed and shorter-lived transit-amplifying cells, tumor formation is halted at early micro-adenoma stages[8]. However, next to this "bottom-up" scenario, additional "top-down" models of intestinal tumorigenesis have been proposed where more committed intestinal cells located at higher positions along the crypt-villus axis are likely to initiate cancer especially in the context of tissue injury and inflammation[9,10]. In the specific case of colon cancer, western style dietary habits and chronic inflammation, two of the major etiologic factors associated with increased risk for sporadic malignant disease in the digestive tract, are thought to induce specific cellular and molecular alterations of the intestinal epithelium which ultimately lead to the expansion of cell targets for tumor initiation and progression[9,11]. However, which specific cell lineages are capable of dedifferentiating upon tissue injury and which are the underlying mechanisms remain largely unclear.

Paneth cells are specialized secretory cells located at the very bottom of the crypt of Lieberkühn in the small intestine where they secrete antimicrobial peptides into the lumen[12]. Moreover, they provide essential physical support and secrete signals to ensure *Lgr5*$^{+}$ stem cell function[13]. In the colon, where Paneth cells are not present, *cKit*$^{+}$ Paneth-like cells, also known as DCS, deep crypt secretory cells, play secretory and niche-like functional roles analogous to those of *bona fide* PCs in the small intestine[14,15].

We first reported on the ability of Paneth cells to re-enter the cell cycle and de-differentiate upon irradiation and inflammation to acquire stem cell-like features and contribute to the tissue regenerative response[1,16,17]. Consequently, we questioned whether Paneth cells could be the origin of intestinal cancer in the context of inflammation. To this aim, we bred mice carrying Lox-alleles at the tumor suppressors and oncogenes most frequently mutated along the adenoma-to-carcinoma sequence, namely *Apc*[18], *Kras*[19], and *Trp53*[20], each combined with a Cre specific for *Lgr5*$^{+}$ CBCs (*Lgr5*$^{CreERT2\text{-}EGFP}$)[21] or for Paneth cells (*Lyz1*^{CreERT2})[22]. Following Cre activation by tamoxifen, DSS was administered through the drinking water to model inflammation (Fig. 1a). In the absence of DSS-induced inflammation, PC-specific single gene mutations did not give rise to intestinal tumors. In contrast, loss of *Apc* in *Lgr5*$^{+}$-CBCs transformed crypts into β-catenin^{hi} foci that grew into multiple adenomas 4-6 weeks after Cre induction (Fig. 1b). When single gene mutations were combined with DSS administration, *Apc* loss in Paneth cells resulted in increased nuclear and cytoplasmic β-catenin expression eventually leading to the formation of PC-derived

61 adenomas (Fig. 1c). Of note, Paneth-specific *Kras* or *Trp53* mutations did not result in tumor formation
62 even in the presence of the inflammatory stimulus (Fig. 1d). However, the compound loss of *Apc* and
63 oncogenic activation of *Kras* in Paneth cells resulted in a striking increase in tumor multiplicity (6.1 fold)
64 even in the absence of DSS (6.9 fold)(Fig. 1e). The combination of *Apc* and *Tp53* mutations in PCs also led
65 to an increase in tumor multiplicity upon DSS administration (1.6 fold), though to a lesser extent when
66 compared with the compound *Apc*/*Kras*-mutant genotype, possibly indicating a distinct mechanism
67 underlying tumor onset in these mice. Indeed, phospho-histone H2A.X (Ser 139) IHC analysis confirmed
68 an increase in DNA damage and chromosomal instability in the *Tp53*-mutant tumors (Suppl. Fig. 1a).
69 Targeting all three genes in Paneth cells resulted in a very aggressive phenotype with high tumor
70 multiplicity (10.1 fold) in the absence of the inflammatory stimulus (Fig. 1e). When compared to *Apc*-
71 driven tumors originated in PCs, the histology of adenomas from mice in which two or three genes were
72 targeted revealed a progressive increase in dysplasia and invasive morphology (Suppl. Fig. 1b).
73 Distribution of adenomas along the small intestine also followed distinct patterns with a prevalence of
74 duodenal tumors in compound *Apc*/*Kras* tumors regardless of DSS (Suppl. Fig. 2a).
75 To validate the Paneth cell origin of the observed intestinal tumors, we bred *Lyz1*^{CreERT2} mice with R26^{LSL-}
76 ^{tdTomato} or R26$^{LSL-YFP}$ reporters and traced their lineage upon tamoxifen-driven targeting of the *Apc, Kras,*
77 and *Tp53* mutations. As shown in Figure 1f and Suppl. Fig. 2b, this confirmed the Paneth cell origin of the
78 corresponding tumors by capturing the process from microscopic lesions to adenoma formation.
79 Overall, these results demonstrate that Paneth cells can initiate intestinal adenomas upon genetic
80 ablation of *Apc* in the context of inflammation. In combination with *Apc* loss, activation of oncogenic *Kras*
81 or loss of *Tp53* function rescues the need for an inflammatory stimulus and results in increased PC-derived
82 tumor multiplicities and progression to malignant phenotype.

83 Next, we characterized lineage-specific markers in the PC- and CBC-originated tumors by
84 immunohistochemistry. Of note, while cells expressing the PC marker lysozyme (Lyz1) were notable in
85 *Lgr5*-derived tumors (*Lgr5*/*Apc*: 30.0 % ± 18.5 positive tumor cells), they were nearly absent in adenomas
86 that originated from Paneth cells (*Lyz1*/*Apc*: 0.48 % ± 1.16)(Fig. 1g-h). The opposite was observed for Dclk1
87 (doublecortin like kinase 1), a Tuft[23] and tumor stem cell marker[24,25], that was more frequently detected
88 among PC-derived adenomas (*Lyz1*/*Apc*: 54.1 % ± 10.5) when compared with *Lgr5*-derived tumors
89 (*Lgr5*/*Apc*: 15.6 % ± 15.7)(Fig. 1i-j). Other lineage-specific markers for entero-endocrine (Chga), goblet
90 (Muc2), and stem cells (Olfm4) showed variable levels without clear-cut differences among tumors with
91 different cells-of-origin (Suppl. Fig. 2c). The increased *Dclk1* expression in PC-derived tumors is of interest
92 in view of its association with increased immune and stromal infiltration in colon cancer[26].

93 To confirm these results at the transcriptional level, expression levels of the *Lyz1* and *Dclk1* genes were
94 analyzed by RTqPCR (Fig. 1k). Indeed, *Lyz1* expression was lower in Paneth-derived tumors (*Lgr5*/*Apc* vs.
95 *Lyz1*/*Apc*: $\log_2$FC = 2.64, P_{val} = 7.5e-4) when compared to *Lgr5*-derived tumors. *Dclk1* expression was very
96 low and variable at the RNA level, and did not show significant differences across the groups.
97 To assess the relative activation levels of the Wnt signaling pathway among the different tumor groups,
98 we measured expression levels of *Axin2*, a well-established Wnt downstream target. *Axin2* expression was
99 higher in *Lgr5*- compared to PC-derived tumors (*Lgr5*/*Apc* vs. *Lyz1*/*Apc*: $\log_2$FC = 2.12, P_{val} = 0.017)(Fig. 1k).
100 Moreover, both *Kras* oncogenic activation and inflammation gradually increased *Axin2* levels in PC-
101 derived tumors, in agreement with the previously reported synergism between *Apc* and *Kras* mutations
102 in the activation of the Wnt pathway[27].
103 Thus, upon tumorigenesis, Paneth cells de-differentiate to a state that hampers secretory
104 differentiation leading to specific patterns of tumor histology and gene expression distinct from that of
105 *Lgr5*-derived tumors.

106 **Paneth cells dedifferentiate into revival stem cells upon enhanced Wnt signaling activation.**
107 To elucidate the mechanisms which underlie the conversion of PCs into cells of origin of small intestinal
108 tumors in the context of inflammation and/or of specific genetic hits, we combined scRNAseq analysis
109 with lineage tracing. To this aim, we induced the *Apc*, *Kras*, and *Tp53* genetic mutations in the R26^{LSL-}
110 ^{tdTomato}/*Lyz1*^{CreERT2} (or R26$^{LSL-YFP}$) reporter strains in the presence or absence of DSS (Fig. 2a). Subsequently,
111 cells were harvested from the intestinal epithelium, purified by FACS, and transcriptionally profiled by
112 scRNAseq (Methods; Suppl. Fig. 3). After preprocessing, we obtained the transcriptomes of 23.231
113 epithelial cells from 32 mice, distributed over the different lineages of the intestinal epithelium (Fig. 2b).
114 Close examination of the cells positive for the reporter genes revealed novel clusters of PCs that arise
115 upon DSS administration and the specific gene mutations, but were not observed among Paneth cells in
116 homeostatic conditions (PC cluster 1-4, Fig. 2c).
117 To characterize the novel PC-derived states, we performed differential expression analysis and identified
118 cluster-specific markers (Fig. 2d)(Suppl. Table 1). While PC Cluster 1 appeared at low frequency across
119 different genotypes, PC Cluster 2 arises directly upon exposure to the inflammatory stimulus. Both PC
120 Clusters 1 and 2 are characterized by increased expression of two markers of radio-resistant and secretory
121 progenitors with self-renewal capacity during regeneration, namely *Krt19*[28] and *Atoh1*[29], while increased
122 expression of *Reg3b*, known for its protective role in the development of colitis and ileitis[30], and *Cdkn1a*
123 (p21), a marker of terminal differentiation in the intestine[31], was observed in Cluster 2 compared to 1.

124 PC Cluster 3 became apparent in mice carrying *Apc* mutations (7.23% ± 5.77 of traced cells) alone and in
125 combination with DSS treatment (16.40% ± 2.10 of traced cells), and in double and triple mutant (AP, AK,
126 AKP) animals, though not in mice carrying single *Kras* or *Tp53* mutations. PC Cluster 3 showed increased
127 expression of *Gif* (gastric intrinsic factor), *Cd81*, a tetraspanin family member known to mark the response
128 to γ–irradiation and correlated with the expression of ISC- and proliferation genes[32], and *Prom1* (prominin
129 1, also known as Cd133), a well-established colon cancer stem cell marker[33].
130 PC Cluster 4 consisted of cells from mice where double (AK) and triple (AKP) mutations were targeted to
131 Paneth cells (23.25% ± 11.23 and 52.26% ± 28.23 of traced cells, respectively). Increased expression of
132 *Anxa2* (annexin 2), a functional marker of inflammatory response, and *Clu* (clusterin), previously shown
133 to earmark revival stem cells (RSCs) upon γ-irradiation[3], feature PC Cluster 4. Accordingly, evaluation of
134 the RSC signature showed elevated expression among the PC clusters (Fig. 2e), and *in situ* hybridization
135 analysis in PC-derived tumors from mice carrying compound mutations (AK and AKP)(Fig. 2f and Suppl.
136 Fig. 4a-b) confirmed the increased *Clu* expression. Finally, pathway analysis revealed the similarities
137 between the PC-derived Cluster 4 and RSCs, both earmarked by the activation of Yap1 signaling and
138 specific inflammatory pathways (Fig. 2g). Compared to RSCs, PC-derived and *Apc/Kras*-mutant cells from
139 Cluster 4 showed increased levels of Tgf-β and Wnt signaling (Suppl. Fig. 4c).
140 Thus, upon genetic targeting or inflammatory stimulus, PCs escape their homeostatic identity and acquire
141 distinct cellular features as shown by scRNAseq and FACS analysis (Suppl. Fig. 4d-e). Of note, DSS
142 treatment led to a lower expression of *Lgr5* and *Ascl2* in stem cells, as well as a lower association of the
143 CBC signature, confirming ours and others' previous observations according to which resident stem cells
144 lose their multipotency upon acute inflammation (Suppl. Fig. 4f)[1].
145 Collectively, these findings demonstrate that PCs efficiently dedifferentiate upon genetic targeting or
146 inflammatory stimulus leading to distinct cellular identities. During tumorigenesis driven by *Apc/Kras*, PCs
147 share features with the Yap1-dependent revival stem cell identity, and further activate Tgf-β and Wnt
148 signaling in their conversion to bona fide tumor cells.

149 **Transcriptomic comparison of Paneth- and *Lgr5*-derived tumors reveals a dichotomy in stem cell**
150 **phenotypes.**

151 To investigate the consequences of the cell-of-origin identity on the transcriptional profile of the
152 resulting intestinal tumors, we performed bulk RNA sequencing of macroscopically dissected lesions
153 originated from ISCs and PCs (Fig. 3a). Principal component analysis revealed that the major variance
154 component (61%) was attributed to differences in the cell-of-origin, while the impact of genotype or
155 inflammatory stimulus became notable in the second component of variation (10%)(Fig. 3b). Differential

156 expression analysis between tumors derived from PCs and ISCs in the same genetic and inflammatory
157 context (*Apc* and DSS) revealed tumor signatures specific for each cell-of-origin (Suppl. Table 2).
158 Gene set enrichment analysis (GSEA) indicated that tumors derived from ISCs were characterized by high
159 levels of Myc and Wnt signaling, while PC-derived adenomas showed higher levels of inflammatory
160 pathways indicative of infiltration from the tumor micro-environment (Fig. 3c, Suppl. Fig. 5). Of note, the
161 inflammatory characteristics of PC-derived tumors were observed also in mice where *Apc* and *Kras*
162 mutations were targeted to Paneth cells in the absence of DSS-driven inflammation (Fig. 3d), indicating
163 that specific mutant genotypes and the type of cell-of-origin can trigger tumor initiation by mimicking the
164 inflammatory context otherwise brought about by DSS.
165 Next, we employed the ISC index[4] (intestinal stem cell index; see Methods) to predict the relative
166 proportions of RSC and CBC stem cells in the intestinal tumors. In agreement with the scRNAseq analysis,
167 PC-derived tumors were RSC-enriched whereas the ISC-derived tumors consisted mainly of CBCs (Fig. 3e).
168 Notably, the highest RSC contribution was observed in tumors originated from *Apc/Kras*-mutant PCs in
169 the absence of inflammation, when compared with the equivalent genotype upon DSS administration.
170 The latter is of relevance to dissect the relative contribution of the inflammatory insult and of the somatic
171 mutations in the de-differentiation process leading to tumor initiation. As mentioned before, one of the
172 primary effects of various forms of tissue injury to the intestinal epithelium is the loss of resident stem
173 cells. In the Singh et al. (2022) study[34], ablation of *Lgr5*$^+$ ISCs was performed to study its consequences by
174 scRNAseq. Our analysis of these data sets revealed elevated expression of secretory genes in the
175 regenerated stem cells normally restricted to the Paneth cell lineage (Suppl. Fig. 6a). In parallel, upon
176 *Lgr5*$^+$ cell ablation, Paneth and goblet cells partially activate the RSC program (Suppl. Fig. 6b), indicating
177 that stem cell loss is sufficient to trigger plasticity and RSC reprogramming from PCs. Hence, in order to
178 assess whether the removal of the resident stem cells is sufficient to activate the lineage tracing capacity
179 of Paneth cells in the absence of the inflammatory injury, we implemented a similar DTR-based *Lgr5*$^+$
180 ablation experiments. As shown in Suppl. Fig. 6c-d, lineage tracing from Paneth cells was observed similar
181 to what previously shown upon inflammation[1].
182 Together, these results indicate that the cell-of-origin embodies the major source of inter-tumor
183 variability, and that the Paneth- or ISC-origin is reflected by the RSC- or CBC-like profile of the resulting
184 tumors, respectively. Notably, the inflammation-driven ISC loss activates de-differentiation at the
185 epithelial level.
186

187 **The transcriptional profile of Paneth-derived tumors mimics colitis-associated colorectal cancer.**

188 The small intestinal location of Paneth cells and of the tumors originating from them raise questions
189 on the relevance of our study for colon cancer, i.e. one of the most frequent cause of morbidity and
190 mortality due to malignancy. To explore the generalizability of our results, we first analyzed bulk and
191 single-cell RNAseq data from two distinct studies[35,36] centered around the AOM/DSS mouse model of
192 colitis-driven colon cancer[37]. This protocol relies on the oncogenic β-catenin mutations caused by
193 azoxymethane (AOM) which, in combination with the DSS-driven ulcerative colitis, result in multiple
194 adenocarcinomas in the distal colon. As shown in Suppl. Fig. 7a (by CiberSortx[38]; see Methods), based on
195 their bulk RNAseq data[35] AOM/DSS-derived colon tumors encompass an abundant population similar to
196 the RSC-like PC Cluster 4. Moreover, analysis of the scRNAseq data[36] confirmed that AOM/DSS-derived
197 colon tumors, when compared to their sporadic counterparts, were distinct in terms of the qualitative
198 and quantitative composition of their tumor microenvironment, namely a pronounced presence of
199 infiltrating immune cells and tumor-associated fibroblasts (Suppl. Fig. 7b). Accordingly, tumor cells derived
200 in the context of AOM/DSS share transcriptional similarity with Paneth-derived tumor cells and RSCs
201 (Suppl. Fig. 7c-d).

202 Hence, notwithstanding the small intestinal location of the PC-derived tumors, their gene expression
203 signatures and overall inflammatory TME profiles are characteristic of colitis-associated carcinoma in the
204 mouse.

205 Next, in view of the marked differences in the transcriptional profiles between mouse intestinal tumors
206 with distinct cells of origin, we questioned whether similar differences distinguish human sporadic colon
207 cancers from those that arose in the context of IBD. To this aim, RNAseq profiles of human microsatellite
208 stable sporadic colorectal cancers (sCRC, N = 38) and from patients suffering from inflammatory bowel
209 disease (IBD-CRC, N = 14) were interrogated[39]. GSEA of the most differentially expressed genes ($log_2FC >$
210 5, $P_{adj} < 0.01$) from the mouse tumors (*Lyz*T signature, N = 27 genes; *Lgr5*T signature, N = 40 genes)
211 revealed a significant association between the *Lyz*T signature and IBD-CRC (NES 1.67, P_{adj} 6.2e-3), while
212 the *Lgr5*T profile was significantly associated with sCRC (NES -1.62, P_{adj} 0.013)(Fig. 3f, Suppl. Fig. 8a-c,
213 Suppl. Table 3). Evaluation of the hallmarks from the molecular signature database[40] revealed gene sets
214 common to PC-derived tumors and IBD-related CRCs (Interferon α/γ, inflammatory response, Il6/Il2
215 signaling, Kras, Complement, Allograft rejection), and to *Lgr5*-derived tumors and sporadic CRCs (Myc
216 targets, G2m Checkpoint, E2F targets and Wnt β-catenin signaling)(Fig. 3g, Suppl. Fig. 8d).

217 We then compared the differentially expressed genes from PC- versus *Lgr5*-derived mouse tumors and
218 human IBD-CRC versus sCRC (Paneth/IBD-CRC, N = 49 genes, Lgr5/sCRC: N = 27 genes) and visualized their

219 expression across different cell types based on a large scRNAseq CRC study[41] (Fig. 3h). Of note, the markers
220 shared between PC-derived tumors and IBD-CRC were dominantly expressed in myofibroblasts (e.g.
221 *ITGAM*, *SLC1A3*), T cells (e.g. *SELPLG, LAX1*), and stromal cells (e.g. *CHRDL1, RELN*). In contrast, *Lgr5*-
222 derived tumors/sCRC markers were mostly observed in epithelial cells (e.g. *HOXB6, HOXB8, HOXB9,*
223 *AXIN2, ASCL2*), indicating the difference in stromal composition among these tumors (Fig. 3h).
224 Comparison of a set of gene signatures (Suppl. Table 4) in a large colorectal cancer cohort[42] confirmed the
225 presence of two distinct identities (Fig. 3i-j): a colitis-like identity enriched with RSCs and prevalent in
226 CMS4 (67%) and CMS1 (36%) tumors, and a sporadic-like identity enriched with CBCs and common in
227 CMS2 (55%) and CMS3 tumors (52%)(Fig. 3k-l, Suppl. Fig. 8e). Survival analysis revealed significant
228 differences in relapse free survival between the sporadic- and colitis-like CRC groups (Pvalue = 5.2e-
229 05)(Fig. 3m). Thus, transcriptional signatures derived from small intestinal mouse tumors originated from
230 Paneth cells significantly overlap with those from human colon cancer that arose in the context of IBD,
231 possibly revealing a common cell-of-origin in secretory lineages.

232 **Western-style diet triggers an inflammatory response in intestinal secretory cells leading to their cell**
233 **cycle activation and dedifferentiation.**

234 The relative representation of patient-derived colon cancers whose expression profiles are reminiscent
235 of the PC-derived mouse tumors (~25%; Figure 3j) vastly exceeds the expected proportion of colon cancers
236 arising in patients with an history of clinically manifest IBD (1-2%)[43]. One possible explanation for this
237 apparent discrepancy may come from the fact that WSD habits, often in combination with chronic over-
238 nutrition and sedentary lifestyles, have been associated with a state of chronic metabolic inflammation,
239 termed 'metaflammation'[44]. In particular, a link between consumption of a diet high in fat and sugar and
240 Paneth cell dysfunction was recently demonstrated[45]. Moreover, in a recent report by J.C. ad L.H.A., a
241 purified mouse diet that mimics WSD habits and underlies the increased risk of colon cancer (NWD1)[46]
242 was shown to induce a low degree of chronic intestinal inflammation and other mechanisms that define
243 pathogenesis of human IBD[47]. Therefore, we hypothesized that etiologic drivers of colon cancer other than
244 IBD, including widespread western-style dietary habits, may underlie dedifferentiation and tumor onset
245 mechanisms similar to those observed upon acute DSS-driven inflammation.

246 To provide support for this hypothesis, we first fed C57BL6/J mice for 3 months with the western-style
247 (NWD1) and control (AIN76A) diets and compared the transcriptional response of Paneth cells with that
248 obtained upon DSS administration (Fig. 4a). We examined genes upregulated upon inflammatory stimuli
249 (DSS signature; see Methods), which showed variable but overall increased levels in NWD1-fed mice when
250 compared to those on the control diet (Fig. 4b). Indeed, GSEA confirmed that the DSS signature was

251 associated significantly with Paneth cells exposed to NWD1 (NES 2.99, $P_{adj} < 0.001$), indicating that
252 western-style dietary habits trigger an inflammatory-like response in Paneth cells (Suppl. Fig. 9a). At the
253 gene ontology level, western-style diet activated signaling pathways related to cell cycle (G2M
254 Checkpoint) and proliferation (mitotic spindle, Myc targets; Suppl. Fig. 9b), suggesting that Paneth cells
255 re-enter the cell cycle upon long-term exposure to western-style diet, similar to what is observed upon
256 DSS-driven inflammation[1].
257 In view of the previously reported acquisition of stem-like features by PCs upon inflammation[1], we next
258 employed the organoid reconstitution assay (ORA)[17,48] to assess whether similar effects are exerted by
259 the western-style diet. We first co-incubated Paneth and *Lgr5*$^{+}$ cells from the AIN76A- and NWD1-fed mice
260 in all 4 combinations. As shown in Figure 4c, Paneth cells from NWD1-fed animals significantly improved
261 organoid formation independently of their reconstitution with *Lgr5*$^{+}$ cells from NWD1- or AIN76A-fed
262 mice, possibly indicative of a paracrine effect enhancing the well-established niche (ISC-supporting) role
263 of Paneth cells. However, single (i.e. non reconstituted with *Lgr5*$^{+}$ CBCs) Paneth cells from NWD1-fed mice
264 formed organoids more efficiently when compared with either PCs from AIN76A-fed mice or with *Lgr5*$^{+}$
265 ISCs from both groups of animals. These *ex vivo* results were further validated by lineage tracing analysis
266 of Paneth cells in R26$^{LSL\text{-}YFP}$*Lyz1*^{CreERT2} NWD1-fed mice that revealed extended YFP-labeled ribbons thus
267 confirming their de-differentiation and acquisition of stem-like features induced by the western-style
268 dietary cues (Fig. 4d).
269 To zoom in on the primary transcriptional response of Paneth cells to NWD1, we took advantage of the
270 scRNAseq data generated by J.C., L.H.C. and collaborators immediately upon exposure to NWD1[47](Fig. 4a).
271 Within 4 days of switching mice to the NWD1 diet, a subset of Paneth cells became apparent whose
272 transcriptional profile strongly associated with the DSS signature (labeled as "diet response cells" in Fig.
273 4e). Mirroring our previous observations obtained immediately upon DSS inflammatory stimulus, these
274 WSD-responsive cells increased their transcriptomic diversity as measured by CytoTRACE[49] (Fig. 4f; see
275 Methods). Already after the short exposure to NWD1, the diet-responsive cells acquired stem cell markers
276 while retaining some secretory features (Fig. 4g). Comparative pathway analysis between the
277 transcriptional response of Paneth cells to DSS and NWD1 revealed similar upregulation of Wnt, Myc,
278 Hedgehog, and G2M checkpoint signaling pathways (Fig. 4h).
279 As the observed WSD-driven gene expression changes are likely exerted through epigenetic modifications,
280 we next analyzed scATAC data obtained in the framework of the same Choi et al. (2023) study[47]. Similar
281 to what observed by scRNAseq analysis, we identified a group of NWD1 diet-responsive Paneth cells with
282 significant epigenetic modifications including a main cluster (52%) on mouse chromosome 11 (synthenic

283 with human chromosomes 17 and 5) that encompasses a considerable fraction of genes encoding for
284 members of the Wnt, Pi3k/Akt and cell cycle pathways (Fig. 4i-k, Suppl. Fig. 9c-f). The latter were
285 previously shown by our laboratory to underlie Paneth cell dedifferentiation and acquisition of stem-like
286 features upon DSS-driven inflammation[1].
287 In order to assess the effects of the NWD1 diet on the mouse colon, we searched for proliferating Paneth-
288 like cells, also known as deep crypt secretory (DCS) cells[14,17]. Inflammation-driven cell cycle activation in
289 these allegedly post-mitotic lineages was previously observed in small intestinal Paneth cells of DSS-
290 treated mice and of Crohn's disease patients[1]. By co-staining colonic tissues with the secretory lineage
291 marker WGA (wheat germ agglutinin)[50] and Ki67, a significant increase in the number of proliferating
292 secretory cells located at the crypt bottom was observed both in mice fed with the NWD1 diet and, as a
293 positive control, in those administered DSS in the drinking water (Fig. 5a-c).
294
295 **Secretory lineages as the cell of origin of human colon cancer**
296 Collectively, our results reveal an alternative bottom-up route to intestinal tumorigenesis originating
297 from Paneth cells in the murine small intestine and, allegedly, from secretory lineages in the human colon,
298 triggered by inflammatory cues as in IBD or through western-style dietary factors. To validate the
299 relevance of our mouse study in patient-derived colon cancer, we took advantage of novel computational
300 methods[5-7] developed to predict the cell of origin of tumors by matching the mutational density along the
301 cancer genome with the profiles of epigenetic modifications characteristic of normal cell types (Suppl. Fig.
302 10a)[51]. While tumors from patients with an IBD history have a similar genome-wide tumor mutational
303 burden compared to their sporadic counterparts (Suppl. Fig. 10b), the presence of regions (genomic
304 windows, see Methods) that are differentially mutated between sCRC and IBD-CRC is suggestive of
305 alternative mutational patterns (Suppl. Fig. 10c-d). Hence, we compared the individual mutational
306 landscapes with the epithelial cell types of the colon to compute the putative cells of origin.
307 As shown in the Fig. 6a (COOBoostR[7], see Methods), while the majority of the sporadic colon cancers
308 appear to originate from stem cells (52%), among the IBD-related cases goblet (40%) and Best4 (28%) cells
309 represent the prevalent cells of origin. Moreover, a substantial proportion of the sporadic cases is also
310 predicted to originate from goblet (22%) and Best4 cells (17%). Best4 cells, named after the specific
311 expression of the bestrophin 4 gene (*BEST4*), form a newly identified and yet only partially characterized
312 intestinal epithelial lineage with dual absorptive and secretory features[52-54]. IHC and scRNAseq analysis in
313 a cohort of ulcerative colitis patients confirmed the presence of actively proliferating goblet and Best4

314 cells (MUC2$^+$ and BEST4$^+$; Fig. 5e-f), indicative of the primary effects of inflammation in these otherwise
315 post-mitotic cells, likely to precede their acquisition of stem-like features.
316 These results are indicative of the fraction of sporadic colon cancers whose expression profiles are
317 reminiscent of the PC-derived tumors and IBD-CRCs (24.7%; Figure 3j). Furthermore, the availability of
318 RNAseq data from a subset of the patient-derived tumors allowed us to confirm the prevalence of RSC-
319 like expression profiles and the high proportion of CMS1 and 4 cases among the sporadic and IBD cases
320 predicted to originate from non-stem, and in particular goblet, cells (Fig. 5g-h, Suppl. Fig. 10e).
321 *Lgr5*$^+$ stem cells have been established as the origin of intestinal tumors[8]. However, whether the same
322 holds true in the context of inflammation has been challenged by their loss of lineage tracing capacity and
323 multipotency upon a broad spectrum of tissue injuries ranging from DSS-driven inflammation[1] to γ-
324 irradiation[16,28], and western-style diet[55]. Our results show that Paneth cell de-differentiation and tumor
325 onset in the mouse small intestine models sporadic colon cancer not only in IBD patients but also in a
326 substantial proportion of the cases predicted to originate in differentiated cell types and not in resident
327 ISCs. Both the differential gene expression profiles and inflammatory and stromal features of the resulting
328 tumors warrant a novel stratification of colon cancer for improved clinical management. Preliminary
329 investigations (*data not shown*) revealed that candidate markers differentially expressed between PC- and
330 *Lgr5*$^+$-initiated mouse tumors such as DCLK1 and HOXB9 were not equally discriminative among patient-
331 derived colon cancers. More systematic and high-throughput screening approaches will likely lead to a
332 novel stratification of the cases based on their cell of origin and specific etiologic factors such as western-
333 style diets and chronic inflammation.
334 Overall, the increased colon cancer risk exerted by inflammation may reflect on a 'trade-off' effect where
335 the chronic nature of the injury continuously stimulates de-differentiation of committed lineages into
336 stem-like cells in support of the tissue's regenerative response, thus resulting in the enlargement of the
337 pool of potential targets for tumor onset. Likewise, the same inflammation-inducing risk factors are bound
338 to affect tumor progression towards malignancy thus resulting into a distinct group of colon cancers with
339 specific prognosis and response to therapy (Fig. 5i).
340 Relative to the debate on the relative contribution of extrinsic risk factors versus the rate of stem cell
341 division to cancer development[56,57], our results indicate that colon cancer etiologic factors such as
342 inflammation and poor dietary habits are likely to result in quantitative and qualitative alterations of the
343 stem cell niche which ultimately predispose to neoplastic transformation. The resulting subset of tumors
344 follow distinct evolutionary paths when compared to Wnt/Myc-driven *Lgr5*-derived tumorigenesis, and

345 are characterized by an inflammatory tumor phenotype more prone to infiltration from the tumor micro-
346 environment.

347 **Methods**

348 **Mice**

349 The following inducible Cre strains encompassing were employed: *Lgr5*$^{CreERT2-EGFP}$ (#008875, Jackson Lab[21])
350 and p*Lys*^{CreERT2} (kind gift from the Clevers Lab[22]). For lineage tracing experiments, mice were crossed with
351 R26$^{LSL-YFP}$ mice (#006148, Jackson Laboratories) or R26$^{LSL-tdTomato}$ mice (#007908, Jackson Laboratories). To
352 target specific mutations in PCs, the above strains were further crossed with *Apc*^{15lox} (#029275, Jackson
353 Laboratories)[18], *Kras*$^{LSL-G12D}$ (#008179, Jackson Laboratories)[19], and *Trp53*^{flox} (#008462, Jackson
354 Laboratories)[20]. For ablation experiments Lgr5$^{DTR-EGFP}$ mice were bred with c-Kit^{CreERT2} and R26$^{LSL-tdTomato}$
355 animals. C-recombinase was activated by intraperitoneal injections of Tamoxifen (1 mg dissolved in 100%
356 EtOH and subsequently in sunflower oil; #T5648 and #S5007, Sigma) once or three times in 4 days. Three
357 days after Tamoxifen injection mice were treated once with diphteria toxin (DT) in order to ablate Lgr5
358 positive cells. To induce acute intestinal inflammation, mice were administered 2-3% dextran sodium
359 sulfate (DSS) in their drinking water for 7 days (#0216011050, MP Biomedicals). DSS-driven inflammation
360 and the corresponding mechanisms underlying the consequent PC dedifferentiation were described in
361 previous studies[1,2,58].For diet experiments, mice were fed with AIN76A or NWD1 diet[55] and collected at
362 various time points (4/8 days, 3/6/9 months). The formulation and composition of the AIN76A and NWD1
363 diets are as outlined in Newmark et al. (Research Diets, New Brunswick, NJ)[46]. In brief, the western diets
364 are based on AIN76A control diet (American Institute of Nutrition76A). NWD1 was adjusted to provide
365 higher fat, and lower vitamin D_3, calcium donors to the single carbon pool and fibre that produces mouse
366 consumption levels similar to those common in segments of western societies with high incidence of
367 colorectal cancer. All mice here employed were inbred C57BL6/J.

368 For all experiments, mice were randomly assigned to experimental groups after matching for gender,
369 age of 8-12 weeks, and genotype. All protocols involving animals were approved by the Dutch Animal
370 Experimental Committee and in accordance with the Code of Practice for Animal Experiments in Cancer
371 Research established by the Netherlands Inspectorate for Health Protections, Commodities and
372 Veterinary Public Health. Animals were bred and maintained in the Erasmus MC animal facility (EDC)
373 under conventional specific pathogen-free conditions.

374

375 **Lineage tracing**

376 *Lys*$^{CreERT2/R26LSL-YFP}$ mice were injected three times with Tamoxifen (1 mg, i.p.) on consecutive days. One
377 week after the last Tamoxifen injection, intestinal tissues were harvested for lineage tracing analysis. To
378 this aim, tissue samples were first dissected and washed with PBS, and then fixed for 2 hours at 25°C with

379 4% buffered formaldehyde solution (Klinipath). Tissues were cryo-protected in 30% sucrose (Sigma)
380 overnight at 4°C, embedded in OCT (KP cryocompound, Klinipath), frozen on dry ice, and sectioned at -
381 20°C. Tissues were cut in 4-8 µm thick sections. These sections were incubated in PBS containing Alexa
382 568 Phalloidin (1:100; Invitrogen) or Alexa 633 Phalloidin (1:100; Invitrogen), and DAPI (Sigma) for 30
383 minutes at 25°C and washed in PBS-T. Tissues were mounted in Vectashield Mounting Medium (Vector
384 Labs) and imaged with a LSM700 confocal microscope (Zeiss). Images were processed with ImageJ.
385 Lineage tracing frequency was quantified by dividing the number of intestinal crypt/villus axes containing
386 Yfp^+ ribbons (encompassing at least 5 Yfp^+ labelled cells) by the total number of counted Yfp labelled
387 crypts. Lineage tracing analysis was performed on 3 mice for each diet type; in each mice at least 60 YFP
388 labelled crypts were analyzed.

389 **Immunohistochemistry on mouse tissues**

390 Tissues were fixed in 4% PFA overnight at 4°C and embedded in paraffin. The 4 µm sections were dewaxed
391 with Xylene and hydrated in consecutive rounds of 70% and 100% EtOH. Antigen retrieval was performed
392 in the 2100 Retriever pressure cooker (BioVendor) at pH 9 with Tris-EDTA buffer. After a 10 minutes
393 incubation at RT with 3% hydrogen peroxidase, tissues were blocked with 5% skim milk powder (Milipore)
394 in PBS-Tween. The following primary antibodies were employed by overnight incubation at 4°C: β-catenin,
395 #610154 (BD Biosciences); γ-H2AX, #9718 (Cell Signaling); Gfp, #A-11122 (ThermoFisher); Olfm4, #D6Y5A
396 (Cell Signaling); Lyz1, #A0099 (Dako); Dclk1, #ab37994 (Abcam); Muc2, #sc-15334 (Santa Cruz); Chga,
397 #NB120-15160 (Novus Bio); Ecad, #610182 (BD Biosciences); Cd3, #ab5690 (Abcam); F4/80, #D2S9R (Cell
398 Signaling); αSMA, #ab5690 (Abcam). Slides were washed twice with PBS-Tween and incubated for 30
399 minutes at room temperature with the Rabbit/Mouse EnVision kits (K4001/K4007, Dako). Slides were
400 counterstained with hematoxylin and, dehydrated with subsequent 70% and 100% EtOH and mounted
401 with Pertex (00811, Histolab). Whole slides were scanned with the Nanozoomer (Hamamatsu) and
402 analyzed with NDP viewer v2 (Hamamatsu).
403

404 **Immunohistochemistry analysis of human tissues**

405 Chromogenic double labelling was performed on 4-µm thick whole slide sections from FFPE tissue blocks,
406 on a validated and accredited automated slide stainer (Benchmark ULTRA System, VENTANA Medical
407 Systems, Tucson, AZ, USA) according to the manufacturer's instructions. Briefly, following
408 deparaffinization and heat-induced antigen retrieval for 40 minutes at 97°C, the tissue samples were
409 incubated with KI67 (MIB-1 antibody, #790-4286; Ventana) for 32 min at 37°C, followed by Ultraview
410 detection (#760-500, Ventana). After the stripping step, MUC2 (CCP58, #M7313, Dako) or BEST4

411 (HPA058564, Sigma-Aldrich) was incubated for 32 min at 37°C and followed by detection with Ultraview
412 Red (#760-501, Ventana) Counterstain was done by hematoxylin II for 12 min and a blue colouring reagent
413 for 8 min. Each tissue slide contained a fragment of FFPE pancreas or tonsil as an on-slide positive control.
414

415 **Immunofluorescence**

416 For cryo-sections, tissue samples were first dissected and washed with PBS, to then be fixed for 2 hours
417 at 25°C with 4% buffered formaldehyde solution (Klinipath). Tissues were cryo-protected in 30% sucrose
418 (Sigma) overnight at 4°C, embedded in OCT (KP cryocompound, Klinipath), frozen on dry ice, and sectioned
419 at −20°C. Tissues were cut in 4-8 µm thick sections. Immunofluorescence was performed using antibodies
420 against Olfm4 (1:200; CST), Mki67 (1:200; Novus biologicals), Lyz1 EC3.2.1.17 (1:1000; Dako), and c-Kit
421 (D13A2)(1:100; CST). Tissue sections were washed and blocked with 5% BSA in PBS-Tween for 1 hour to
422 then be incubated with the primary antibody overnight at 4°C. Slides were washed twice with PBS-Tween
423 and slides were incubated for 2 hours with Goat anti-Rabbit IgG (H+L) secondary Antibody, Alexa Fluor®
424 488 conjugate, (1:250; Life Technologies) and Wheat Germ Agglutinin (WGA)™ 647 conjugate (1:500,
425 ThermoFisher Scientific). Tissues were counterstained with DAPI (Sigma) and where indicated with F-actin
426 (#SC001, Spirochrome) for 30 min. at 25°C and washed in PBS-T. Tissues were mounted in VECTASHIELD
427 HardSet Antifade Mounting Medium (Vector Labs) and imaged with a Zeiss LSM700 confocal microscope.
428

429 ***In situ* hybridization**

430 In situ hybridization was performed by RNAscope™ Multiplex Fluorescent V2 Assay (ACDBio) technology
431 in combination with the RNA-Protein Co-Detection kit (ACDBio), according to the manufacturer's
432 instructions. In brief, 4 µm paraffin embedded sections were dehydrated, blocked for 10 minutes at room
433 temperature with H_2O_2, and processed with 1X Antigen Retrieval co-detection buffer for 15 minutes at
434 99°C. Sections were incubated with Ecad (1:250, #610182, BD Biosciences) overnight at 4°C. Hybridization
435 was performed with a probe targeting mouse *Clu* (Cat#427891, ADCBio), and the probe signal was
436 developed with Vivid dye 520 nm (1:1500). Sections were counterstained by DAPI and anti-mouse Alexa
437 633 (1:250, Invitrogen) and mounted with ProLong™ Gold Mountant (ThermoFisher). Samples were
438 imaged on the Stellaris 5 Confocal Microscope (Leica) and images were processed with ImageJ.
439

440 **Image analysis**

441 Images were scanned by Nanozoomer and imported in QuPath[59] as IHC images. Within intestinal tumors,
442 regions of interest (ROI) were randomly assigned and consisted of 300-600 cells. Next, the ROIs were

443 processed with positive cell selection plugin using default settings based on Cell DAB OD mean. The
444 percentage of positive cells per ROI was exported and visualized in R, where statistical tests were
445 performed. Fluorescent images were processed with ImageJ.
446
447 **Quantification of Ki67/WGA cells in murine colon**
448 The percentage of $Ki67^+/WGA^+$ double positive cells was quantified by dividing double positive cells by the
449 total amount of WGA^+ in the lower half of the colonic crypt. Only clearly detectable double positive cells,
450 as determined by the analysis of z-stacks were counted. For each quantification, at least 30 crypts of at
451 least 3 experimental mice were employed.
452
453 **Quantitative real-time PCR**
454 RNA was converted into cDNA using the High Capacity RNA-to-cDNA kit (Applied Biosystems). Samples
455 were run in duplicates on the 7500 Real Time system (Applied Biosystems). Quantitative PCR was
456 performed using the TaqMan assay (Applied Biosystems) according to instructions of the manufacturer.
457 Samples were normalized to the beta-actin (*Actb*) house-keeping gene. The gene-specific Taqman probes
458 were: Mm02619580_g1 (*Actb*), Mm00443610_m1 (*Axin2*), Mm00657323 (*Lyz1*), Mm01545303 (*Dclk1*).
459 Data were processed and visualized in R and statistical tests were employed to assess significance with
460 one-way ANOVA and Tukey post hoc test.
461
462 **Isolation of mouse intestinal crypts and cell dissociation**
463 Mouse small intestines were flushed with cold PBS, removed from fat and scraped with a glass slide to
464 remove intestinal villi. Resected sample were then sectioned into 5-10 mm segments and washed with
465 cold PBS before incubation for 30 minutes at 4°C in cold PBS supplemented with 6 mM EDTA. After an
466 additional PBS wash, crypts were detached from the muscle layer by 4 rounds of harsh pipetting with cold
467 PBS. Crypts were treated for 10 minutes at room temperature with DNAse (2000 U/ml-1, Thermo
468 Scientific) in Advanced DMEM/F-12 medium and passed through a 70 µm strainer. Purified crypts were
469 dissociated with 1 mL of pre-warmed TryplE and DNAse for 3 minutes at 37°C. Single cells were pelleted
470 in 10 mL ADF, resuspended in 3 mL 5% FCS HBSS and manually counted.
471
472 **Fluorescence activated cell sorting**
473 Cell suspensions were blocked with TruStain Fc blocking reagent (Biolegend) for 10 minutes at 4°C. After
474 washing with 5% FCS HBSS, cells were stained for 30 minutes at 4°C in 100 µl with Lin antibodies (CD31-

475 BV421 #563356, CD45-BV421 #563890, TER119-BV421 #563998, BD Biosciences), CD24-APC (#1109070,
476 Sony Biotechnology), and cKit-PE (#105808, Biolegend). For scRNAseq experiments, the antibody mix was
477 supplemented with 2 µl Hashing Antibody (Biolegend TotalSeq^{TM} Hashtag antibodies: #155831, #155833,
478 #155837, #155843, #155849) to label the cells with oligo barcodes. After 3 washes with 3.5 mL 5% FCS
479 HBSS, cells were filtered with a 40 µm strainer and resuspended in 1 mL 5% FCS HBSS with 1 µg/mL DAPI
480 (D9542, Sigma-Aldrich). FACS analysis and sorting were performed using a FACSAriaIII (BD Biosciences).
481 DAPI and BV421-conjugated antibodies were detected using a 405nm laser and 450/40 BP filter. GFP and
482 BB515-conjugated antibodies were detected using a 488nm laser and 502LP + 530/30 BP filters. tdTomato
483 and PE-conjugated antibodies were detected using a 561nm laser and 582/15 BP filter. APC-conjugated
484 antibodies were detected using a 633nm laser and 660/20 BP filter. Samples were sorted for epithelial
485 (Lin^{neg}), Paneth-enriched (SSC^{hi}CD24^{hi}cKit^{hi}), and traced cells (Yfp^{hi}/td-Tomato^{hi}) according to previously
486 established gates[1,16,17]. To optimize the sorting for single cell experiments, the initial single cell gate was
487 followed by a more stringent, population specific single cell gate[16]. FACS strategy was visualized with
488 FlowJo V10.
489
490 **Organoid Reconstitution Assay**
491 Whole crypts were extracted from the small intestine of *Lgr5*-EGFP mice fed for 3 month (from weaning)
492 with either AIN76A or NWD1 diets[55]. After cellular dissociation and FACS, single *Lgr5*$^{+}$ and Paneth cells
493 were sorted in separate Eppendorf LoBind Tubes. Reconstitution of *Lgr5*-EGFP^{hi} stem cells with PCs
494 (SSC^{hi}CD24^{hi}cKit^{hi}) was performed by co-pelleting sorted cells at 300 g for 5 minutes in Eppendorf LoBind
495 Tubes, and by incubating them for 15 minutes at 25°C as previously described[17,48]. The cells were then
496 resuspended in 30 µL Matrigel (Corning), and cultured in 96 Well Flat Bottom dishes (Corning).
497 Additionally, Paneth and Lgr5 positive cells were plated singularly where indicated and cultured in
498 standard ENR medium[60] supplemented with 10 µM Y-27632 (Sigma) and 1 mM Jagged-1 (AnaSpec). Cells
499 were plated in triplicates and the generated organoids where counted 9 days after plating. Experiments
500 were repeated at 3 independent moments.
501
502 **Droplet-based scRNAseq**
503 Sorted single cells were mixed in equal sample proportions to a pool of 25-50k cells in 5% FCS HBSS to a
504 final concentration of ±1000 cells/µl. The cell pool was recounted manually with Trypan blue and between
505 10-15k cells were loaded into a 10X Genomics Chip (Next GEM Chip G). The Gel Bead-In EMulsions were
506 generated with the Chromium Controller (10X Genomics) using Single Cell 3' v3 chemistry with

507 FeatureBarcoding. After generation of cDNA and quality check with Bioanalyzer (Agilent), libraries were
508 sequenced with the Novaseq 6000 (Illumina) till a depth of 20-40k reads/cell. Raw data was processed
509 with CellRanger count (cellranger-7.0.0)[61] and aligned to the mm10 mouse reference genome with the
510 addition of the transgenes Yfp and Td-tomato.
511
512 **Analysis of scRNAseq: inflammation and genetic targeting of Paneth cells**
513 For each single cell run, filtered gene-cell matrices were imported in R using Seurat (v 4.1.1)[62]. After a
514 centered log ratio transformation (CLR) of the hashtag oligo counts, cells were assigned back to their
515 mouse of origin using HTODemux (positive quantile = 0.99). Cells assigned as doublets or negative for any
516 of the barcodes were filtered from the data. Cells from mice with different gender but same genotype and
517 experimental group were further separated based on the expression *Xist*. After preprocessing, the five
518 runs were merged into a single Seurat object. To remove putative doublets from the sorting, doublets
519 were simulated and called by doubletfinder_v3 (nExp = 0.01)[63]. After removal of doublets, low quality cells
520 were removed by filters based on the percentage of mitochondrial genes (> 10%), on nFeature_RNA (<
521 200), and nCount_RNA (< 500). Next, data were integrated with the single cell transform (SCT) pipeline
522 using reciprocal PCA dimension reduction to find integration anchors. Integrated data was further
523 processed by dimension reduction with Uniform Manifold Approximation and Projection (UMAP) on the
524 first 30 principal components. Cells were clustered using shared nearest neighbor (SNN) modularity
525 optimization (resolution = 0.6) and annotated according to canonical marker genes. Traced cells were
526 defined as cell with a non-zero value for either td-Tomato or Yfp. Signatures were evaluated using the
527 Addmodulescore function and visualized in experimental groups or cell clusters using Violin Plots.
528 Pathway level evaluation was done using the GSVA package[64] on summarized expression profiles using
529 Average Expression by cell cluster.
530
531 **Bulk RNAseq of intestinal tumors**
532 Intestinal tumors were macro-dissected from intestinal tissues and cut into 1-2 mm small fragments which
533 were then re-suspended in 500 µl TRIzol (#15596026, Ambion) for RNA isolation. RNA quality was first
534 evaluated by Nanodrop ND-1000 (ThermoFisher) and further purified with the TURBO DNA-free Kit
535 (Invitrogen). Samples were sequenced with a read length of 150 bp (PE150) using the DNA nanoball (DNB-
536 seq) protocol till a depth of 25M reads/sample (BGI, Hong Kong). Adapter trimming and sequencing QC
537 was performed with SOAPnuke software[65] .
538

539 **Analysis of Lyz1/Lgr5-derived mouse tumors: bulk RNAseq**

540 The FASTQ files were aligned with STAR (v2.7.9a) to the mm10 mouse reference genome with Ensemble
541 gene annotations[66]. After alignment, Sambamba (0.8.0) was applied to mark duplicates and perform
542 flagstat quality checks[67]. Next, Subread (2.0.3) was used to count the primary strand-specific alignment[68].
543 Downstream analysis was performed in R using the DeSeq2 package (v 1.34.0)[69]. In brief, counts were log2
544 normalized and used for principal component analysis on the top 500 variable expressed genes.
545 Differential expression analysis was done following the DeSeq pipeline with Negative Binomial GLM fitting
546 and Wald statistics and genes were filtered using $\log_2$FC >1.5, $P_{adj} < 0.01$. Gene set enrichment analysis
547 was done with the fgsea package (v 1.20.0) using the HallMarks gene modules from the molecular
548 signature database[40]. Gene set variation analysis was performed using the GSVA package (v 1.42.0)[64]. The
549 relative proportion of RSC/CBC stem cell types was computed with the ISC index using default settings[4].

550

551 **Analysis of Paneth cells upon exposure to inflammation and western-style diet: bulk RNAseq**

552 The FASTQ files were removed from TrueSeq adapters using Trimmomatic (v0.36). STAR[66] was used to
553 align the reads to the mm10 reference genome using Gencode annotation release M15 (GRCm38.p5).
554 Mapping quality was assessed with Sambamba Flagstat statistics. Count files were generated using
555 FeatureCounts (subread) and further processed in R using the DeSeq2 package. Differential expression
556 analysis were performed between the groups 'NWD1 diet' (n = 3) vs. 'AIN76 diet' (n = 3) with the Wald-
557 test. A heat map was produced using z-score scaled data and visualized with the ComplexHeatmap
558 package (v2.12.1).

559

560 **Analysis of IBD-CRC and sCRC RNAseq cohort**

561 RNA-seq material was previously described in Rajamäki et al.[39] In brief, 64 CRCs entered HiSeq LncRNA-
562 Seq library preparation and paired-end sequencing using Illumina HiSeqXTen. Salmon (version 0.12.0;
563 quant mode with ValidateMappings) was used to map raw sequences onto the human transcriptome
564 (Ensembl release 79). Gene-level quantification was done with DESeq2 (v1.18.1) followed by a variance
565 stabilizing transformation and Limma (v3.34.9) correction of sequencing batch effects[69]. Only
566 microsatellite stable (MSS) tumors were included in the analyses. Differential gene expression was
567 calculated as ANOVA between 38 MSS sCRCs and 14 MSS IBD-CRCs. GSVA (v1.42.0)[64] analyses were ran
568 using default options (Gaussian kernel) and predefined gene sets from the molecular signature database[40].
569 Conensus Molecular Subtypes were mapped to the samples with the random forest classifier of
570 CMSClassifier R package.

571

572 **Cell of origin predictions from IBD-CRCs/sCRCs**

573 *Processing of Whole-Genome Sequencing (WGS) data of CRCs*

574 DNA was isolated from fresh-frozen tumor, normal colon, or blood. Paired tumor-normal WGS data was
575 generated from altogether 25 MSS IBD-CRCs and 257 MSS sCRCs. Libraries were prepared using TruSeq
576 Nano DNA HT or TruSeq PCR-Free Kit (Illumina), followed by paired-end sequencing using Illumina
577 platform (HiSeqXTen/HiSeq2000). More details are given in Rajamäki et al.[39]. Sequence alignment to the
578 GRCh38 reference genome, other data preprocessing steps, and somatic variant calling were performed
579 with GenomeAnalysisToolkit GATK4 best practices workflow (version 4.0.4.0)[70]. Mutations were filtered
580 based on allele fraction (AF) to extract clonal somatic variants. A genome-wide mean and standard
581 deviation was calculated for each tumor; somatic variants were then filtered to a minimum AF of one
582 standard deviation below the mean. On average, 85% of variants per tumor (IQR 83%-87%) were kept-in
583 as clonal somatic variants for the subsequent analysis. Similar to previous work[5,6], the human reference
584 genome (hg38) was processed in non-overlapping windows of 1 million base pairs. We excluded window-
585 regions with <92% of bases within uniquely mapped 36-mers, regions overlapping telomeres and
586 centromeres and regions outside autosomes. Altogether 2387 windows remained for the analysis. To
587 identify differentially mutated windows, patients were normalized by the average of their windows and
588 IBD-CRCs vs sCRCs were compared with an Wilcoxon Rank Sum test ($P < 0.01$).

589

590 *Processing of scATAC data from human colon*

591 Normal colon (N = 9) samples from Becker et al.[51] were obtained from the public domain under GEO
592 identifier GSE201349. Signac[71] was used for processing and the FeatureMatrix function was used to
593 generate a count matrix based on the previously described 2387 windows. Cell labels were retrieved from
594 the original publication and reduced to 6 major classes by the aggregation of clusters from the same cell
595 type. To generate the embedding, batch correction was performed with IntegrateData, and UMAP was
596 computed on the 2:30 latent semantic indexing (LSI) components. To generate the chromatin mark
597 features per cell type, the counts from the scATAC data set were grouped with the AggregateExpression
598 function and equalized to 10M reads per cell type.

599

600 *Predictions with COOBoostR*

601 COOBoostR[7], an extreme gradient boosting-based (XGBoost) machine learning algorithm designed for the
602 prediction of cells of origin, was used to predict the putative cells of origin for each individual sample from

603 the WGS cohort (N = 282 tumors) based on the epigenetic profiles from the human colonic scATAC data.
604 We ran the algorithm with default values from XGBoost for the learning rate (mEta = 0.3) and the
605 maximum depth of the trees (mdepth = 6). Tumor predictions were aggregated on cohort level, and IBD-
606 CRC/sCRC were compared with a Fisher's exact test. For a subset of patients (N = 48 tumors), WGS and
607 RNAseq was available. Hence, for these tumors, CMS labels and signatures from the gene set variation
608 analysis (GSVA) were compared based on stratification by putative cell of origin.
609
610 **Analysis of human CRC bulk RNAseq cohort**
611 Log2 normalized expression of the meta cohort described in Guinney et al.[42] was obtained from the R2
612 Genomics Analysis and Visualization Platform and subsequently processed in R. Gene set variation analysis
613 was performed with the GSVA package using the Gaussian kernel[64]. Subsequently, correlations of the gene
614 signatures (Suppl. Table 4) were visualized with ggcorr using Pearson Correlation. Next, samples were
615 classified as colitis-like, sporadic-like or as intermediate based on their GSVA scores for the IBD-CRC and
616 sCRC signatures. Using this classification, samples were visualized with their annotated Consensus
617 Molecular Subtype (CMS). Survival analysis was performed with the survival and survminer packages in R.
618 Multivariate analysis was performed with the log-rank test and pairwise comparisons were fitted with a
619 Cox proportional hazards regression model.
620
621 **Analysis of human scRNAseq cohorts**
622 *Colorectal cancer data set*
623 Filtered count matrices were retrieved from the gene expression omnibus (KUL cohort: GSE144735; SMC
624 cohort: GSE132465)[41] and processed in R with Seurat. After normalization and scaling of the Seurat object,
625 gene expression was summarized per cell type using AverageExpression based on the overlapping
626 differentially expressed genes of murine (Paneth vs. *Lgr5*) and human (IBD-CRC vs. sCRC) tumor groups.
627 The average expression was z-scored and visualized as a heat map using the ComplexHeatmap package.
628
629 *Ulcerative Colitis data set*
630 Data from Smillie et al.[52] was processed with the Seurat[62] workflow. A subset was taken encompassing
631 the epithelial cells according to annotation from the authors. Cells were defined as positive when they
632 had non-zero counts for that particular gene. Cells were aggregated on patient level and a t-test was
633 performed to compare number of double and single positive cells across the UC (N = 17) and control group
634 (N = 12).

635

636 **Analysis of mouse intestinal single cell data sets**

637 *Homeostasis and γ-irradiation*

638 Count matrices from Haber et al.[72] and Ayyaz et al.[3] were downloaded from GEO using GSE92332 and
639 GSE117783, respectively. After preprocessing using the Seurat workflow, Seurat objects were merged and
640 gene expression was averaged by cell type and study using AverageExpression. Next, gene set variation
641 analysis (GSVA)[64] was computed using the Gaussian kernel and the output was visualized in a heat map
642 using the ComplexHeatmap package.

643

644 *AIN76A and NWD1 diets: scRNAseq*

645 The intestinal epithelia of mice fed with control (AIN76A) and western-style diets (4 days NWD1, 4 days
646 NWD1 + 4 days AIN recovery) were collected and sent for 10X Genomics scRNAseq analysis (N = 3 mice
647 per group)[47]. After preprocessing with Seurat and batch correction using the integrated assay workflow,
648 the Seurat clusters were annotated according to canonical markers. CytoTRACE[49] was computed on the
649 whole data set using default settings. Next, Paneth cells (N = 991 cells) were taken from the data set, sub-
650 clustered, and visualized by UMAP with a split by the dietary condition. The DSS signature was computed
651 using AddModuleScore and projected on the UMAP embedding. The Paneth sub-cluster that appeared in
652 the NWD1 conditions and associated with the DSS signature was relabeled as 'Diet response'. Next,
653 marker genes were visualized using ViolinPlot based on the separation of diet response PCs and other PCs.
654 Last, Paneth cells from the diet data set were merged with the Paneth cells from the DSS data set. Average
655 expression was computed based on experimental condition, and GSVA analysis (Gaussian kernel) was
656 performed using the predefined gene sets from the Molecular Signature Database (Hallmark set)[40,64]. A
657 filter was applied to select pathways that were both upregulated in DSS and NWD1 condition (ΔGSVA =
658 0.2). The output was visualized as heat map using the ComplexHeatmap package.

659

660 *AIN76A and NWD1 diets: scATACseq*

661 The intestinal epithelia of mice fed with control (AIN76A) and western-style diets (3 months) were
662 collected and sent for 10X Genomics scATACseq analysis (N = 2 mice per group)[47]. Processing was done
663 with Signac[71], and UMAP embedding was produced base on the 2:30 latent semantic indexing (LSI)
664 components. Unsupervised clustering was performed by a shared nearest neighbor (SNN) modularity
665 optimization based clustering algorithm (algorithm: 1, resolution: 1.2). Cell type predictions scores were
666 obtained by the integration with the AIN76A/NWD1 scRNAseq data set using the FindTransferAnchors

667 and TransferData functions. Two out of twenty-one clusters had high association to the Paneth cell
668 prediction score (cluster 5,20). Paneth cells were defined as part of either cluster 5/20 with the additional
669 condition of a non-zero prediction score for Paneth cells. Next, Paneth cells (N = 945 cells) were taken
670 from the data set, and visualized by UMAP with a split by the dietary condition. Cluster 5 represented cells
671 from both diets while cluster 20 was enriched in NWD1 and therefore relabeled as 'Diet response'. To
672 identify differentially accessible peaks, FindMarkers was used with logistic regression test. Peaks were
673 filtered based on $P < 0.05$, visualized with a RegionHeatmap and RIdeogram on the mouse genome, and
674 gene ontology was performed on the closest genes using the EnrichR prackage.
675
676 *Lgr5 ablation with Diphtheria toxin*
677 Count matrices were obtained from GEO (GSE183299) and processing was done with the Seurat
678 workflow[62]. The revival stem cell (RSC) signature was evaluated using the Addmodulescore function and
679 visualized across experimental groups and cell clusters using the ComplexHeatmap package. A subset was
680 made of intestinal stem cells, and differential expression analysis was performed with FindMarkers. The
681 results were visualized with the EnhancedVolcano package, where marker genes of Paneth cells were
682 highlighted.
683
684 *AOM/DSS-derived tumors*
685 Data from Vega et al.[36] was downloaded through GEO (GSE134255) and processed with Seurat[62].
686 Differential abundance analysis was performed with MiloR[73] workflow using default parameters. The
687 revival stem cell (RSC) signature and the PC Cluster 4 signature were evaluated using the Addmodulescore
688 function and visualized with ViolinPlots.
689
690 **CiberSortx analysis of AOM/DSS adenomas**
691 CiberSortx[38] was leveraged to predict the fractions of various cell types in tumors arising in AOM/DSS
692 context. To this aim, count data from AOM/DSS-derived adenomas from Chen et al.[35] (GSE178145) were
693 converted to counts per million with Edger. The single cell count data from Paneth cell upon genetic
694 targeting were provided as reference and converted to a signature matrix in CiberSortx using default
695 parameters. For cell type imputation, CiberSortx was applied in relative mode using 100 permutations.
696
697 **Data availability**

698 All data relevant to this study are made available. Transcriptomic sequencing data has been deposited in
699 the Gene Expression Omnibus (GEO), and is available using the following identifiers: GSE221819 (bulk RNA
700 sequencing of murine tumors); GSE221820 (single cell RNA sequencing of genetically targeted Paneth
701 cells); GSE221818 (bulk RNA sequencing of sorted Paneth cells treated with control and western-style
702 diet). Additional data sets referenced in this study are publicly available in the Synapse and GEO
703 repositories. Previously published scRNAseq studies were employed relative to the mouse small intestine
704 in homeostasis (Haber et al.[72], GSE92332), upon irradiation (Ayyaz et al.[3], GSE117783), *Lgr5* ablation (Singh
705 et al.[34] GSE183299), and upon feeding with western-style diet (Choi et al. [47], scRNAseq: GSE188577,
706 scATACseq: GSE228006). Mouse colonic scRNAseq data from AOM/DSS tumors was obtained from Vega
707 et al. [36] (GSE134255) and bulk RNAseq was from Chen et al.[35] (GSE178145). Human colorectal cancer Bulk
708 RNAseq and scRNAseq studies were retrieved from Guinney et al.[42] (syn2623706), Rajamäki et al.[39] and
709 Lee et al.[41] (KUL cohort: GSE144735; SMC cohort: GSE132465), respectively. Human scRNAseq data from
710 Ulcerative Colitis patients (Smillie et al.[52]) was downloaded from the Broad DUOS platform after a DTA
711 agreement. Single cell ATAC data from human colon was obtained from Becker et al.[51] (GSE201349).
712

713 **Figure Legends**

714 **Figure 1. Paneth cells as the cell-of-origin of intestinal cancer.**

715 **a.** Cre-Lox strategy taimed at the targeting of *Apc*, *Kras*, and *Tp53* mutations in intestinal stem cells (*Lgr5*$^+$
716 ISCs) and Paneth cells (*Lyz1*$^+$ PCs). **b.** and **c.** β-catenin IHC analysis of intestinal tumors initiated from *Lgr5*$^+$
717 ISCs (**b**) and PCs (**c**). The asterisks indicate *Lgr5*$^+$ ISCs and PCs with enhanced cytoplasmic and nuclear β-
718 catenin accumulation; tumor foci and adenomas are indicated by dashed lines. **d-e.** Tumor multiplicity
719 was calculated according to tumor-bearing animals (**d**) and by tumor number per genotype (**e**) in the
720 presence/absence of DSS and based on Swiss roll counts. Error bars denote standard deviations of the
721 mean. P values denote one-way ANOVA and Tukey post-hoc tests for group comparisons. **f.** Lineage
722 tracing analysis of Paneth cells (labelled by YFP) at different stages of tumor-initiation and progression. **g-**
723 **j.** Left panels: Lyz1 (**g**) and Dclk1 (**i**) IHC analysis *Lgr5*$^+$ ISCs and PCs-derived adenomas. Top-right inlets (**h-**
724 **j**): quantification of number of *Lyz1*- (**h**) and *Dclk1*-positive (**j**) tumor cells. P values depict one-way ANOVA
725 and Tukey post-hoc tests for group comparisons. **k.** *Lyz1*, *Dclk1*, and *Axin2* qPCR expression analysis across
726 different adenoma genotypes. P values represent one-way ANOVA and Tukey post-hoc tests for group
727 comparisons.

728

729 **Figure 2. Paneth cells dedifferentiate into a revival stem cell (RSC) identity.**

730 **a.** Schematics of the experimental approach. After genetic targeting of Paneth cells, intestinal crypts were
731 extracted, and the isolated cells labeled with hashing antibodies and sorted according to three different
732 sorting strategies: epithelium, PC-enriched and PC-traced cells. **b.** UMAP embedding of the different cell
733 clusters/lineages (left panel), annotated according to the expression of canonical marker genes (right
734 panel). **c.** Bar plot of the distribution of traced cells across the different mouse genotypes and
735 experimental conditions. **d.** Violin plots representing marker genes of the newly identified Paneth-derived
736 cell clusters (PC Cluster 1-4). **e.** Association analysis of the revival stem cell (RSC) signature with PC Cluster
737 1-4. **f.** RNA *in situ* hybridizations of the *Clu* gene in small tumors derived from Paneth cells upon compound
738 targeting of *Apc* and *Kras* mutations. **g.** Gene sets variation analysis among the Haber et al.[72], Ayyaz et
739 al.[3], and the present studies.

740

741 **Figure 3. Paneth-derived adenomas have an inflammatory phenotype mimicking colitis-associated**
742 **colon cancer.**

743 **a**. Schematics of the experimental approach to compare PC- and *Lgr5*-derived adenomas. **b**. Principal
744 Component Analysis (PCA) plot showing that the cell-of-origin is the dominant discriminator of variance.

745 **c**. Bar plot summarizing the gene set enrichment analysis between Paneth- (*Lyz1 Apc* DSS) and ISC- (*Lgr5*
746 *Apc* DSS) derived tumors. Pathways were filtered based on Pval < 0.05 and abs NES > 0.5. **d**. Subset of
747 inflammatory pathways, visualized as heat map based on values from the gene set variation analysis. **e**.
748 Box plots showing results of the stem cell index. P value depicts result of one-way ANOVA. **f**. Gene set
749 enrichment analysis showing significant but opposite association between the *Lyz1* tumor signature and
750 IBD-CRCs, and between the *Lgr5* tumor signature and sCRC. **g**. Heatmap showing GSVA scores, averaged
751 per tumor group, of pathways with similar patterns between the murine and human tumor groups. **h**.
752 Heatmap highlighting the differentially expressed genes (log2FC >1.5, Padj < 0.01) shared between the
753 Paneth/IBD-tumors and the *Lgr5*/sCRC-tumors. Values denote z-scores of average expression per cell
754 type. **i-m**. Two distinct sporadic colon cancer identities become apparent upon analysis of a large cohort
755 of CRC tumors (N = 3232 samples). **i.** Heatmap showing Pearson Correlations of the GSVA scores. **j-k**.
756 Scatter plot showing two distinct clusters of sporadic- and colitis-like in all (**j**) colon cancers and (**k**)
757 stratified according to their consensus molecular subtype (CMS). Grey lines indicate contours lines,
758 dashed lines show thresholds to classify tumors in colitis-like, sporadic-like, and intermediate groups. **l**.
759 Stacked bar plot analysis showing the distribution of consensus molecular subtypes (CMS1 to 4) across
760 the colitis-like and sporadic-like colon cancers. **m**. Kaplan-Meier survival analysis for relapse free survival.
761 P values denote result of log-rank test and cox regression models for univariate analyses. Hazard ratios
762 (HR) and confidence intervals (CI) are displayed for pairwise comparisons.
763
764 **Figure 4. Western-style diet triggers an inflammatory response leading to Paneth cell dedifferentiation.**
765 **a.** Schematics of the experimental approach designed to investigate the consequences of short- and long-
766 term exposure to western-style diet (NWD1) vs. control (AIN76A) diets. **b**. Heatmap showing z-scored DSS
767 signature (DSS vs. Control; Padj < 0.05, Log2FC > 0.25) in Paneth cells exposed to DSS or NWD1. **c**. Organoid
768 multiplicities derived either from single ISCs or PCs, and from reconstituted doublets (L: Lgr5+ ISCs, P:
769 Paneth cells). Pooled data from N = 4 independent experiments. P values were calculated using one-way
770 ANOVA and Tukey tests for group comparisons. Error bars depict standard deviations from the mean. **d**.
771 Representative image of lineage tracings from a NWD1-fed Lyz1-Yfp mouse. Scale bar: 50 µm. P value
772 depicts result of the student t-test and error bar represents the standard deviation. Data from N = 3 mice.
773 **e**. UMAP showing Paneth cells from AIN76A- and NWD1-fed mice (N = 3 mice per condition). The DSS
774 signature portrayed on UMAP embedding, highlights a subcluster of Paneth cells responsive to the NWD1
775 diet. **f**. Violin plots showing different levels of the DSS signature (top) and CytoTRACE score (bottom)
776 between the PCs responsive to the NWD1 diet and other Paneth cells. P values depict significance values

777 of Wilcoxon test. **g**. Violin plots representing marker genes of PCs responsive to the NWD1 diet, showing
778 co-expression of stem and secretory markers. **h**. Heatmap visualization of gene set variation analysis,
779 indicating pathways that are activated in Paneth cells after exposure to DSS or NWD1. **i**. UMAP plot of
780 Paneth cell subset in scATAC data set of AIN (N = 2) and NWD1 (N = 2) treated mice. **j**. Heat map listing
781 differential peaks between Diet response Paneth cells and other PCs. **k**. Ideogram displaying the
782 distribution along the mouse chromosomes of the differential peaks observed upon diet response (red)
783 cell when compared to those characteristic of Paneth cells (blue).
784
785 **Figure 5. Inflammation activates distinct cells of origin in the colon.**
786 **a.** Colonic tissues from either untreated mice or from mice administered 3% DSS for 7 days, as well as
787 from mice fed with the AIN76A or NWD1 synthetic diets for 3 months were analyzed for the presence of
788 proliferative deep crypt secretory (DSC) cells. WGA (wheat germ agglutinin) was used to stain DSC cells[50],
789 and Ki67 to mark proliferative cells. Tissues were counterstained by DAPI (nucleus). Asterisks mark
790 WGA/Ki67 double positive cells. **b-c**. Quantification of WGA^+/$Ki67^+$cells (**b**) and total WGA^+ cells (**c**) in the
791 lower colonic crypt of the mice, as shown in (**a**). Scale bar = 20 µm. A minimum of 50 crypts from 3 different
792 mice were analysed. **d**. Barplot showing the predicted cell-of-origin in a cohort of IBD-CRC (N = 25) and
793 sCRC (N = 257)[39] based on the COOBoostR computational approach[7] (see Methods). P value depicts result
794 of the Fisher exact test. **e**. MUC2, BEST4, and Ki67 IHC analysis of colonic tissues obtained from controls
795 and IBD patients. Asteriks mark examples of double positive cells. **f**. Boxplot showing percentage of cycling
796 ($Ki67^+$) $MUC2^+$ and $REG4^+$ cells in Ulcerative Colitis patients and controls. scRNAseq data are from Smillie
797 et al.[52]. Positivity was defined per cell by the presence of at least one read for that particular marker.
798 Subsequently, cells were aggregated per patient to calculate percentages. **g**. Box plot denoting differences
799 in the stem cell index based on stratification of predicted cell-of-origin in a subset of IBD-CRC and sCRC
800 cases for which RNAseq data were available[39]. P value depict the result of the t-test. **h**. Mapping of
801 Consensus Molecular Subtypes (CMS) on tumor samples stratified according to their predicted cell-of-
802 origin. P value depicts result of the Fisher exact test. **i**. Graphic abstract of the model arising from the
803 present study. Colon cancer can be initiated either from stem (CBC) or differentiated cells, the latter in
804 response to inflammatory cues. RSC reprogramming is activated in support of the regenerative response.
805 During this process, actively dividing RSCs expand the cell targets for tumor initiation and progression,
806 leading to an alternative route to tumorigenesis earmarked by an inflammatory phenotype.
807
808

809 **Supplementary Figure Legends**

810 **Supplementary Figure 1. Immuno-histologic analysis of Paneth-derived tumors.**

811 **a.** Representative IHC images of Paneth-derived tumors from different genetic backgrounds, stained with
812 phospho-histone H2A.X (Ser 139). **b.** Top three panels: IHC analysis of Paneth-derived intestinal tumors
813 with different genetic backgrounds (as indicated), stained for β-catenin. Bottom: hematoxylin and eosin
814 histological stains of Paneth-derived tumors from *Lyz1*/*Apc*/*Kras*/*Tp53* mice.

815

816 **Supplementary Figure 2. Characterization of PC-derived small intestinal adenomas.**

817 **a**. Stacked bar plot displaying the localization and distribution of PC-derived adenomas across the small
818 intestine. **b**. Immunofluorescence imaging of intestinal crypts from *Lyz1*/tdTomato and *Lyz1-AK*/tdTomato
819 mice. **c**. IHC analysis of the lineage-specific ChgA, Muc2, and Olfm4 markers in PC- and *Lgr5*-derived
820 adenomas.

821

822 **Supplementary Figure 3. FACS gating strategy for Paneth cells enrichment and isolation.**

823 **a.** FACS gating strategy established for the isolation of live, single, epithelial cells (top). Subsequently,
824 Paneth cells were enriched using the $SSC^{hi}CD24^{hi}$ gate and further purified based on high cKit levels
825 ($SSC^{hi}CD24^{hi}cKit^{hi}$). Alternatively, traced cells were sorted based on positive expression for Yfp or td-
826 Tomato when the appropriate reporter mice were employed. **b.** Negative control employed to establish
827 reference levels based on unstained samples. **c.** Bar plot of the percentage of Paneth cells obtained by the
828 distinct gating strategies. P values depict results of one-way ANOVA and Tukey tests.

829

830 **Supplementary Figure 4. Paneth cells dedifferentiate upon DSS-driven inflammation.**

831 **a-b.** In situ hybridization (ISH) analysis of Clu mRNA (green) expression at various stages during PC-derived
832 tumorigenesis in *Lyz1-Apc*/*Kras* and (**b**) *Lyz1-Apc*/*Kras*/*Tp53* mice. **c.** Bar plot showing filtered pathways
833 (Pval < 0.05, abs NES > 0.5) of the gene set enrichment analysis comparing RSCs with PC Cluster 4. **d.** FACS
834 analysis of lineage-traced (Yfp+) cells in wild type (*Lyz1*-Yfp) and AKP-mutant (*Lyz1-Apc*/*Kras*/*Tp53*) mice.
835 The latter clearly localize outside of the $CD24^{hi}cKit^{hi}$ gate where wild type PCs reside. **e.** Bar plot relative
836 to the percentages of lineage-traced cells evaluated by FACS using the $CD24^{hi}cKit^{hi}$ PC-specific gate (left),
837 or by scRNAseq analysis (% within Paneth cluster; right). P values denote significance of one-way ANOVA.
838 **f.** Left: Bar plots showing the average percentage of *Ascl2*$^{+}$ and *Lgr5*$^{+}$ stem cells in control and DSS-treated
839 animals. Right: Violin plots showing a decrease in the crypt base columnar (CBC) signature upon DSS
840 treatment. P values denote significance of one-way ANOVA and Tukey test for group comparisons.

841

842 **Supplementary Figure 5. Distinct TME features in CBC- and PC-derived small intestinal adenomas.**

843 IHC analysis of *Lgr5*$^{+}$- and *Lyz*-derived adenomas with the tumor microenvironment markers αSMA
844 (fibroblasts), F4/80 (macrophages), and Cd3 (T cells).

845

846 **Supplementary Figure 6. *Lgr5*$^{+}$ CBCs ablation triggers dedifferentiation of Paneth and goblet secretory**
847 **lineages.**

848 **a.** Differential expression analysis of intestinal stem cells in homeostasis and during regeneration
849 following *Lgr5*$^{+}$ CBCs ablation. scRNAseq are from Singh et al.[34]. Several among the top 50 differentially
850 expressed genes in the regenerated ISCs are Paneth-specific markers (red). **b**. Heatmap showing
851 transcriptional activity of the RSC program upon *Lgr5*$^{+}$ CBCs ablation. **c-d**. Lineage tracing of DT-treated
852 *Lgr5*$^{DTR\text{-}EGFP}$;*c-Kit*^{CreERT2}; Rosa^{tdTomato} mice across different intestinal sections (c.) and double stained with
853 Lyz1/tdTomato (d.). Scale bar = 50 µM, 2 mice per group were analyzed.

854

855 **Supplementary Figure 7. AOM/DSS-derived adenomas share similarities with PC-derived tumors.**

856 **a**. Stacked bar plot of the cell type fractions in AOM/DSS adenomas as predicted by Cibersort analysis[38]
857 (see Methods). Bulk RNAseq data are from Chen et al.[35]. **b**. Differential cell type abundance (MiloR[73]; see
858 Methods) between AOM/DSS and *Lrig1-Apc* adenomas. scRNAseq data are from Vega et al.[36]. **c**.
859 Comparison of RSC and PC Cluster 4 module score in tumor cells from AOM/DSS and *Lrig1-Apc* adenomas.
860 **d**. Venn diagram indicating the overlap between marker genes from PC Cluster 4 and the AOM/DSS-
861 specific squamous tumor cell subpopulation.

862

863 **Supplementary Figure 8. Differential gene expression analysis between IBD colon cancers and murine**
864 **PC-derived small intestinal adenomas.**

865 **a**. Volcano plot showing differentially expressed (Pval < 0.01, FC cutoff 1.5) genes between *Lgr5*- and
866 Paneth-derived intestinal tumors. **b**. Volcano plot highlighting differentially expressed (Pval < 0.01, FC
867 cutoff 1) genes between sporadic- and IBD-CRCs. **c**. Box plots relative to differentially expressed CBC (Lgr5-
868 derived) and RSC (PC-derived) marker genes between sporadic- and IBD-CRCs. P values denote results of
869 the t test. **d**. Bar plot relative to the gene set enrichment analysis between sCRC and IBD-CRC (abs NES >
870 0.5, Pval < 0.05). **e**. Box plots relative to stem cell index values across the colitis, sporadic, and intermediate
871 group of colon cancers. P value depicts result of one-way ANOVA.

872

873 **Supplementary Figure 9. The NWD1 western-style diet triggers the dedifferentiation of Paneth cells.**
874 **a**. GSEA plot of Paneth cells from NWD1- vs. AIN76A-fed mice. The DSS signature significantly associates
875 with the NWD1 diet (NES 2.99, Padj 2.5e-56). **b**. Bar plot showing pathways elevated ($P < 0.05$, $NES > 0.5$)
876 in Paneth cells from NWD1- when compared to AIN76A-fed animals. **c**. Prediction scores for Paneth (left)
877 and goblet (right) cells on UMAP embedding from the scATAC data (Choi et al.[47]). **d**. Unsupervised
878 clustering reveals two distinct clusters (c5, c20) that include Paneth cells. **e**. Bar plot listing gene ontology
879 results based on differential peaks from the diet responsive Paneth cells. **f**. Immunofluorescence imaging
880 of WGA and Olf4m showing intestinal crypts from mice fed with AIN/NWD1 diets. Asterisks earmark
881 double positive cells. Scale bar indicates 10 µm.
882
883 **Supplementary Figure 10. Epigenetic profiles of normal colonic lineages and mutational patterns of IBD-**
884 **related and sporadic colon cancers.**
885 **a**. UMAP plot displaying 1 Mb processed scATAC data of the human colon (Becker et al.[51]). **b**. Average
886 number of passenger mutations in IBD-related and sporadic colon cancers[39]. **c**. Relative mutation
887 frequency in IBD-enriched (N = 78) and sCRC-enriched (N = 136) bins based on Wilcox test ($p<0.01$). **d**.
888 Barplot showing the genomic overview of differential bins across chromosomes. **e**. Boxplots relative to
889 the gene set variation analysis (GSVA) scores of tumors stratified according to their predicted cell of origin.
890 P values denote results of t tests.

891 **References**

892 1. Schmitt, M., Schewe, M., Sacchetti, A., Feijtel, D., van de Geer, W. S., Teeuwssen, M., Sleddens, H. F.,
893 Joosten, R., van Royen, M. E., van de Werken, H. J. G., van Es, J., Clevers, H. & Fodde, R.2018 Paneth
894 Cells Respond to Inflammation and Contribute to Tissue Regeneration by Acquiring Stem-like Features
895 through SCF/c-Kit Signaling. *Cell Rep* **24**, 2312-2328 e2317, doi:S2211-1247(18)31203-8 [pii]
896 10.1016/j.celrep.2018.07.085.
897 2. Yu, S., Tong, K., Zhao, Y., Balasubramanian, I., Yap, G. S., Ferraris, R. P., Bonder, E. M., Verzi, M. P. &
898 Gao, N.2018 Paneth Cell Multipotency Induced by Notch Activation following Injury. *Cell Stem Cell* **23**,
899 46-59 e45, doi:10.1016/j.stem.2018.05.002.
900 3. Ayyaz, A., Kumar, S., Sangiorgi, B., Ghoshal, B., Gosio, J., Ouladan, S., Fink, M., Barutcu, S., Trcka, D.,
901 Shen, J., Chan, K., Wrana, J. L. & Gregorieff, A.2019 Single-cell transcriptomes of the regenerating
902 intestine reveal a revival stem cell. *Nature* **569**, 121-125, doi:10.1038/s41586-019-1154-y
903 10.1038/s41586-019-1154-y [pii].
904 4. Vasquez, E. G., Nasreddin, N., Valbuena, G. N., Mulholland, E. J., Belnoue-Davis, H. L., Eggington, H. R.,
905 Schenck, R. O., Wouters, V. M., Wirapati, P., Gilroy, K., Lannagan, T. R. M., Flanagan, D. J., Najumudeen,
906 A. K., Omwenga, S., McCorry, A. M. B., Easton, A., Koelzer, V. H., East, J. E., Morton, D., Trusolino, L.,
907 Maughan, T., Campbell, A. D., Loughrey, M. B., Dunne, P. D., Tsantoulis, P., Huels, D. J., Tejpar, S.,
908 Sansom, O. J. & Leedham, S. J.2022 Dynamic and adaptive cancer stem cell population admixture in
909 colorectal neoplasia. *Cell Stem Cell* **29**, 1213-1228 e1218, doi:S1934-5909(22)00303-4 [pii]
910 10.1016/j.stem.2022.07.008.
911 5. Kübler, K., Karlić, R., Haradhvala, N. J., Ha, K., Kim, J., Kuzman, M., Jiao, W., Gakkhar, S., Mouw, K. W.,
912 Braunstein, L. Z., Elemento, O., Biankin, A. V., Rooman, I., Miller, M., Karthaus, W. R., Nogiec, C. D.,
913 Juvenson, E., Curry, E., Kenudson, M. M.-., Ellisen, L. W., Brown, R., Gusev, A., Tomasetti, C., Lolkema,
914 M. P., Steeghs, N., Herpen, C. v., Kim, H.-G., Lee, H., Vlahoviček, K., Bernstein, B. E., Sawyers, C. L.,
915 Hoadley, K. A., Cuppen, E., Koren, A., Arndt, P. F., Louis, D. N., Stein, L. D., Foulkes, W. D., Polak, P.,
916 Getz, G., Pathology, o. b. o. t. P., Clinical Correlates Working Group & Network, t. I. T. P.-C. A. o. W.
917 G.2019 Tumor mutational landscape is a record of the pre-malignant state. *bioRxiv*, 517565,
918 doi:10.1101/517565.
919 6. Polak, P., Karlic, R., Koren, A., Thurman, R., Sandstrom, R., Lawrence, M., Reynolds, A., Rynes, E.,
920 Vlahovicek, K., Stamatoyannopoulos, J. A. & Sunyaev, S. R.2015 Cell-of-origin chromatin organization
921 shapes the mutational landscape of cancer. *Nature* **518**, 360-364, doi:10.1038/nature14221.

922 7. Yang, S., Ha, K., Song, W., Fujita, M., Kubler, K., Polak, P., Hiyama, E., Nakagawa, H., Kim, H. G. & Lee,
923 H.2022 COOBoostR: An Extreme Gradient Boosting-Based Tool for Robust Tissue or Cell-of-Origin
924 Prediction of Tumors. *Life (Basel)* **13**, doi:life13010071 [pii] life-13-00071 [pii] 10.3390/life13010071.
925 8. Barker, N., Ridgway, R. A., van Es, J. H., van de Wetering, M., Begthel, H., van den Born, M., Danenberg,
926 E., Clarke, A. R., Sansom, O. J. & Clevers, H.2009 Crypt stem cells as the cells-of-origin of intestinal
927 cancer. *Nature* **457**, 608-611, doi:nature07602 [pii] 10.1038/nature07602.
928 9. Schwitalla, S., Fingerle, A. A., Cammareri, P., Nebelsiek, T., Goktuna, S. I., Ziegler, P. K., Canli, O.,
929 Heijmans, J., Huels, D. J., Moreaux, G., Rupec, R. A., Gerhard, M., Schmid, R., Barker, N., Clevers, H.,
930 Lang, R., Neumann, J., Kirchner, T., Taketo, M. M., van den Brink, G. R., Sansom, O. J., Arkan, M. C. &
931 Greten, F. R.2013 Intestinal tumorigenesis initiated by dedifferentiation and acquisition of stem-cell-
932 like properties. *Cell* **152**, 25-38, doi:10.1016/j.cell.2012.12.012.
933 10. Shih, I. M., Wang, T. L., Traverso, G., Romans, K., Hamilton, S. R., Ben-Sasson, S., Kinzler, K. W. &
934 Vogelstein, B.2001 Top-down morphogenesis of colorectal tumors. *Proc Natl Acad Sci U S A* **98**, 2640-
935 2645, doi:10.1073/pnas.051629398 051629398 [pii].
936 11. Li, W., Zimmerman, S. E., Peregrina, K., Houston, M., Mayoral, J., Zhang, J., Maqbool, S., Zhang, Z., Cai,
937 Y., Ye, K. & Augenlicht, L. H.2019 The nutritional environment determines which and how intestinal
938 stem cells contribute to homeostasis and tumorigenesis. *Carcinogenesis* **40**, 937-946,
939 doi:10.1093/carcin/bgz106.
940 12. Bevins, C. L. & Salzman, N. H.2011 Paneth cells, antimicrobial peptides and maintenance of intestinal
941 homeostasis. *Nat Rev Microbiol* **9**, 356-368, doi:10.1038/nrmicro2546.
942 13. Sato, T., van Es, J. H., Snippert, H. J., Stange, D. E., Vries, R. G., van den Born, M., Barker, N., Shroyer,
943 N. F., van de Wetering, M. & Clevers, H.2011 Paneth cells constitute the niche for Lgr5 stem cells in
944 intestinal crypts. *Nature* **469**, 415-418, doi:10.1038/nature09637.
945 14. Rothenberg, M. E., Nusse, Y., Kalisky, T., Lee, J. J., Dalerba, P., Scheeren, F., Lobo, N., Kulkarni, S., Sim,
946 S., Qian, D., Beachy, P. A., Pasricha, P. J., Quake, S. R. & Clarke, M. F.2012 Identification of a cKit(+)
947 colonic crypt base secretory cell that supports Lgr5(+) stem cells in mice. *Gastroenterology* **142**, 1195-
948 1205 e1196, doi:S0016-5085(12)00171-0 [pii] 10.1053/j.gastro.2012.02.006.
949 15. Sasaki, N., Sachs, N., Wiebrands, K., Ellenbroek, S. I., Fumagalli, A., Lyubimova, A., Begthel, H., van den
950 Born, M., van Es, J. H., Karthaus, W. R., Li, V. S., Lopez-Iglesias, C., Peters, P. J., van Rheenen, J., van
951 Oudenaarden, A. & Clevers, H.2016 Reg4+ deep crypt secretory cells function as epithelial niche for
952 Lgr5+ stem cells in colon. *Proc Natl Acad Sci U S A* **113**, E5399-5407, doi:1607327113 [pii]
953 10.1073/pnas.1607327113.

954 16.Roth, S., Franken, P., Sacchetti, A., Kremer, A., Anderson, K., Sansom, O. & Fodde, R.2012 Paneth cells
955 in intestinal homeostasis and tissue injury. *PLoS One* **7**, e38965, doi:10.1371/journal.pone.0038965.
956 17.Schewe, M., Franken, P. F., Sacchetti, A., Schmitt, M., Joosten, R., Bottcher, R., van Royen, M. E.,
957 Jeammet, L., Payre, C., Scott, P. M., Webb, N. R., Gelb, M., Cormier, R. T., Lambeau, G. & Fodde, R.2016
958 Secreted Phospholipases A2 Are Intestinal Stem Cell Niche Factors with Distinct Roles in Homeostasis,
959 Inflammation, and Cancer. *Cell Stem Cell* **19**, 38-51, doi:10.1016/j.stem.2016.05.023.
960 18.Robanus-Maandag, E. C., Koelink, P. J., Breukel, C., Salvatori, D. C., Jagmohan-Changur, S. C., Bosch, C.
961 A., Verspaget, H. W., Devilee, P., Fodde, R. & Smits, R.2010 A new conditional Apc-mutant mouse
962 model for colorectal cancer. *Carcinogenesis* **31**, 946-952, doi:10.1093/carcin/bgq046.
963 19.Jackson, E. L., Willis, N., Mercer, K., Bronson, R. T., Crowley, D., Montoya, R., Jacks, T. & Tuveson, D.
964 A.2001 Analysis of lung tumor initiation and progression using conditional expression of oncogenic K-
965 ras. *Genes Dev* **15**, 3243-3248, doi:10.1101/gad.943001.
966 20.Marino, S., Vooijs, M., van Der Gulden, H., Jonkers, J. & Berns, A.2000 Induction of medulloblastomas
967 in p53-null mutant mice by somatic inactivation of Rb in the external granular layer cells of the
968 cerebellum. *Genes Dev* **14**, 994-1004, doi:https://www.ncbi.nlm.nih.gov/pubmed/10783170.
969 21.Barker, N., van Es, J. H., Kuipers, J., Kujala, P., van den Born, M., Cozijnsen, M., Haegebarth, A., Korving,
970 J., Begthel, H., Peters, P. J. & Clevers, H.2007 Identification of stem cells in small intestine and colon by
971 marker gene Lgr5. *Nature* **449**, 1003-1007, doi:10.1038/nature06196.
972 22.van Es, J. H., Wiebrands, K., Lopez-Iglesias, C., van de Wetering, M., Zeinstra, L., van den Born, M.,
973 Korving, J., Sasaki, N., Peters, P. J., van Oudenaarden, A. & Clevers, H.2019 Enteroendocrine and tuft
974 cells support Lgr5 stem cells on Paneth cell depletion. *Proc Natl Acad Sci U S A*,
975 doi:10.1073/pnas.1801888117.
976 23.Gerbe, F., van Es, J. H., Makrini, L., Brulin, B., Mellitzer, G., Robine, S., Romagnolo, B., Shroyer, N. F.,
977 Bourgaux, J. F., Pignodel, C., Clevers, H. & Jay, P.2011 Distinct ATOH1 and Neurog3 requirements define
978 tuft cells as a new secretory cell type in the intestinal epithelium. *J Cell Biol* **192**, 767-780,
979 doi:10.1083/jcb.201010127.
980 24.Nakanishi, Y., Seno, H., Fukuoka, A., Ueo, T., Yamaga, Y., Maruno, T., Nakanishi, N., Kanda, K.,
981 Komekado, H., Kawada, M., Isomura, A., Kawada, K., Sakai, Y., Yanagita, M., Kageyama, R., Kawaguchi,
982 Y., Taketo, M. M., Yonehara, S. & Chiba, T.2013 Dclk1 distinguishes between tumor and normal stem
983 cells in the intestine. *Nat Genet* **45**, 98-103, doi:10.1038/ng.2481.
984 25.Westphalen, C. B., Asfaha, S., Hayakawa, Y., Takemoto, Y., Lukin, D. J., Nuber, A. H., Brandtner, A.,
985 Setlik, W., Remotti, H., Muley, A., Chen, X., May, R., Houchen, C. W., Fox, J. G., Gershon, M. D., Quante,

986 M. & Wang, T. C.2014 Long-lived intestinal tuft cells serve as colon cancer-initiating cells. *J Clin Invest*
987 **124**, 1283-1295, doi:73434 [pii] 10.1172/JCI73434.
988 26.Wu, X., Qu, D., Weygant, N., Peng, J. & Houchen, C. W.2020 Cancer Stem Cell Marker DCLK1 Correlates
989 with Tumorigenic Immune Infiltrates in the Colon and Gastric Adenocarcinoma Microenvironments.
990 *Cancers (Basel)* **12**, doi:10.3390/cancers12020274.
991 27.Janssen, K. P., Alberici, P., Fsihi, H., Gaspar, C., Breukel, C., Franken, P., Rosty, C., Abal, M., El Marjou,
992 F., Smits, R., Louvard, D., Fodde, R. & Robine, S.2006 APC and oncogenic KRAS are synergistic in
993 enhancing Wnt signaling in intestinal tumor formation and progression. *Gastroenterology* **131**, 1096-
994 1109, doi:S0016-5085(06)01750-1 [pii] 10.1053/j.gastro.2006.08.011.
995 28.Asfaha, S., Hayakawa, Y., Muley, A., Stokes, S., Graham, T. A., Ericksen, R. E., Westphalen, C. B., von
996 Burstin, J., Mastracci, T. L., Worthley, D. L., Guha, C., Quante, M., Rustgi, A. K. & Wang, T. C.2015
997 Krt19(+)/Lgr5(-) Cells Are Radioresistant Cancer-Initiating Stem Cells in the Colon and Intestine. *Cell*
998 *Stem Cell* **16**, 627-638, doi:S1934-5909(15)00171-X [pii] 10.1016/j.stem.2015.04.013.
999 29.Castillo-Azofeifa, D., Fazio, E. N., Nattiv, R., Good, H. J., Wald, T., Pest, M. A., de Sauvage, F. J., Klein, O.
1000 D. & Asfaha, S.2019 Atoh1(+) secretory progenitors possess renewal capacity independent of Lgr5(+)
1001 cells during colonic regeneration. *EMBO J* **38**, doi:embj.201899984 [pii] EMBJ201899984 [pii]
1002 10.15252/embj.201899984.
1003 30.Shindo, R., Katagiri, T., Komazawa-Sakon, S., Ohmuraya, M., Takeda, W., Nakagawa, Y., Nakagata, N.,
1004 Sakuma, T., Yamamoto, T., Nishiyama, C., Nishina, T., Yamazaki, S., Kameda, H. & Nakano, H.2020
1005 Regenerating islet-derived protein (Reg)3beta plays a crucial role in attenuation of ileitis and colitis in
1006 mice. *Biochem Biophys Rep* **21**, 100738, doi:S2405-5808(19)30332-2 [pii] 100738 [pii]
1007 10.1016/j.bbrep.2020.100738.
1008 31.Gartel, A. L., Serfas, M. S., Gartel, M., Goufman, E., Wu, G. S., el-Deiry, W. S. & Tyner, A. L.1996 p21
1009 (WAF1/CIP1) expression is induced in newly nondividing cells in diverse epithelia and during
1010 differentiation of the Caco-2 intestinal cell line. *Exp Cell Res* **227**, 171-181, doi:S0014-4827(96)90264-
1011 5 [pii] 10.1006/excr.1996.0264.
1012 32.Sato, T., Sase, M., Ishikawa, S., Kajita, M., Asano, J., Sato, T., Mori, Y. & Ohteki, T.2020 Characterization
1013 of radioresistant epithelial stem cell heterogeneity in the damaged mouse intestine. *Sci Rep* **10**, 8308,
1014 doi:10.1038/s41598-020-64987-1 [pii] 64987 [pii] 10.1038/s41598-020-64987-1.
1015 33.Ricci-Vitiani, L., Lombardi, D. G., Pilozzi, E., Biffoni, M., Todaro, M., Peschle, C. & De Maria, R.2007
1016 Identification and expansion of human colon-cancer-initiating cells. *Nature* **445**, 111-115,
1017 doi:nature05384 [pii] 10.1038/nature05384.

1018 34.Singh, P. N. P., Madha, S., Leiter, A. B. & Shivdasani, R. A.2022 Cell and chromatin transitions in
1019 intestinal stem cell regeneration. *Genes Dev* **36**, 684-698, doi:gad.349412.122 [pii]
1020 10.1101/gad.349412.122.
1021 35.Chen, L., Luo, Z., Zhao, C., Li, Q., Geng, Y., Xiao, Y., Chen, M. K., Li, L., Chen, Z. X. & Wu, M.2022 Dynamic
1022 Chromatin States Coupling with Key Transcription Factors in Colitis-Associated Colorectal Cancer. *Adv*
1023 *Sci (Weinh)* **9**, e2200536, doi:ADVS4194 [pii] 10.1002/advs.202200536.
1024 36.Vega, P. N., Nilsson, A., Kumar, M. P., Niitsu, H., Simmons, A. J., Ro, J., Wang, J., Chen, Z., Joughin, B.
1025 A., Li, W., McKinley, E. T., Liu, Q., Roland, J. T., Washington, M. K., Coffey, R. J., Lauffenburger, D. A. &
1026 Lau, K. S.2022 Cancer-Associated Fibroblasts and Squamous Epithelial Cells Constitute a Unique
1027 Microenvironment in a Mouse Model of Inflammation-Induced Colon Cancer. *Front Oncol* **12**, 878920,
1028 doi:10.3389/fonc.2022.878920.
1029 37.Tanaka, T., Kohno, H., Suzuki, R., Yamada, Y., Sugie, S. & Mori, H.2003 A novel inflammation-related
1030 mouse colon carcinogenesis model induced by azoxymethane and dextran sodium sulfate. *Cancer Sci*
1031 **94**, 965-973, doi:10.1111/j.1349-7006.2003.tb01386.x.
1032 38.Steen, C. B., Liu, C. L., Alizadeh, A. A. & Newman, A. M.2020 Profiling Cell Type Abundance and
1033 Expression in Bulk Tissues with CIBERSORTx. *Methods Mol Biol* **2117**, 135-157, doi:10.1007/978-1-
1034 0716-0301-7_7.
1035 39.Rajamaki, K., Taira, A., Katainen, R., Valimaki, N., Kuosmanen, A., Plaketti, R. M., Seppala, T. T.,
1036 Ahtiainen, M., Wirta, E. V., Vartiainen, E., Sulo, P., Ravantti, J., Lehtipuro, S., Granberg, K. J., Nykter, M.,
1037 Tanskanen, T., Ristimaki, A., Koskensalo, S., Renkonen-Sinisalo, L., Lepisto, A., Bohm, J., Taipale, J.,
1038 Mecklin, J. P., Aavikko, M., Palin, K. & Aaltonen, L. A.2021 Genetic and Epigenetic Characteristics of
1039 Inflammatory Bowel Disease-Associated Colorectal Cancer. *Gastroenterology* **161**, 592-607, doi:S0016-
1040 5085(21)00680-6 [pii] 10.1053/j.gastro.2021.04.042.
1041 40.Subramanian, A., Tamayo, P., Mootha, V. K., Mukherjee, S., Ebert, B. L., Gillette, M. A., Paulovich, A.,
1042 Pomeroy, S. L., Golub, T. R., Lander, E. S. & Mesirov, J. P.2005 Gene set enrichment analysis: a
1043 knowledge-based approach for interpreting genome-wide expression profiles. *Proc Natl Acad Sci U S*
1044 *A* **102**, 15545-15550, doi:0506580102 [pii] 10.1073/pnas.0506580102.
1045 41.Lee, H. O., Hong, Y., Etlioglu, H. E., Cho, Y. B., Pomella, V., Van den Bosch, B., Vanhecke, J., Verbandt,
1046 S., Hong, H., Min, J. W., Kim, N., Eum, H. H., Qian, J., Boeckx, B., Lambrechts, D., Tsantoulis, P., De
1047 Hertogh, G., Chung, W., Lee, T., An, M., Shin, H. T., Joung, J. G., Jung, M. H., Ko, G., Wirapati, P., Kim, S.
1048 H., Kim, H. C., Yun, S. H., Tan, I. B. H., Ranjan, B., Lee, W. Y., Kim, T. Y., Choi, J. K., Kim, Y. J., Prabhakar,
1049 S., Tejpar, S. & Park, W. Y.2020 Lineage-dependent gene expression programs influence the immune

1050 landscape of colorectal cancer. *Nat Genet* **52**, 594-603, doi:10.1038/s41588-020-0636-z
1051 10.1038/s41588-020-0636-z [pii].
1052 42.Guinney, J., Dienstmann, R., Wang, X., de Reynies, A., Schlicker, A., Soneson, C., Marisa, L., Roepman,
1053 P., Nyamundanda, G., Angelino, P., Bot, B. M., Morris, J. S., Simon, I. M., Gerster, S., Fessler, E., De
1054 Sousa, E. M. F., Missiaglia, E., Ramay, H., Barras, D., Homicsko, K., Maru, D., Manyam, G. C., Broom, B.,
1055 Boige, V., Perez-Villamil, B., Laderas, T., Salazar, R., Gray, J. W., Hanahan, D., Tabernero, J., Bernards,
1056 R., Friend, S. H., Laurent-Puig, P., Medema, J. P., Sadanandam, A., Wessels, L., Delorenzi, M., Kopetz,
1057 S., Vermeulen, L. & Tejpar, S.2015 The consensus molecular subtypes of colorectal cancer. *Nat Med*
1058 **21**, 1350-1356, doi:nm.3967 [pii] 10.1038/nm.3967.
1059 43.Munkholm, P.2003 Review article: the incidence and prevalence of colorectal cancer in inflammatory
1060 bowel disease. *Aliment Pharmacol Ther* **18 Suppl 2**, 1-5, doi:10.1046/j.1365-2036.18.s2.2.x.
1061 44.Christ, A., Lauterbach, M. & Latz, E.2019 Western Diet and the Immune System: An Inflammatory
1062 Connection. *Immunity* **51**, 794-811, doi:S1074-7613(19)30416-9 [pii] 10.1016/j.immuni.2019.09.020.
1063 45.Liu, T. C., Kern, J. T., Jain, U., Sonnek, N. M., Xiong, S., Simpson, K. F., VanDussen, K. L., Winkler, E. S.,
1064 Haritunians, T., Malique, A., Lu, Q., Sasaki, Y., Storer, C., Diamond, M. S., Head, R. D., McGovern, D. P.
1065 B. & Stappenbeck, T. S.2021 Western diet induces Paneth cell defects through microbiome alterations
1066 and farnesoid X receptor and type I interferon activation. *Cell Host Microbe* **29**, 988-1001 e1006,
1067 doi:S1931-3128(21)00180-3 [pii] 10.1016/j.chom.2021.04.004.
1068 46.Newmark, H. L., Yang, K., Kurihara, N., Fan, K., Augenlicht, L. H. & Lipkin, M.2009 Western-style diet-
1069 induced colonic tumors and their modulation by calcium and vitamin D in C57Bl/6 mice: a preclinical
1070 model for human sporadic colon cancer. *Carcinogenesis* **30**, 88-92, doi:10.1093/carcin/bgn229.
1071 47.Choi, J., Zhang, X., Li, W., Houston, M., Peregrina, K., Dubin, R., Ye, K. & Augenlicht, L.2023 Dynamic
1072 Intestinal Stem Cell Plasticity and Lineage Remodeling by a Nutritional Environment Relevant to Human
1073 Risk for Tumorigenesis. *Mol Cancer Res* **21**, 808-824, doi:726118 [pii] MCR-22-1000 [pii] 10.1158/1541-
1074 7786.MCR-22-1000.
1075 48.Schewe, M., Sacchetti, A., Schmitt, M. & Fodde, R.2017 The Organoid Reconstitution Assay (ORA) for
1076 the Functional Analysis of Intestinal Stem and Niche Cells. *J Vis Exp*, doi:56329 [pii] 10.3791/56329.
1077 49.Gulati, G. S., Sikandar, S. S., Wesche, D. J., Manjunath, A., Bharadwaj, A., Berger, M. J., Ilagan, F., Kuo,
1078 A. H., Hsieh, R. W., Cai, S., Zabala, M., Scheeren, F. A., Lobo, N. A., Qian, D., Yu, F. B., Dirbas, F. M.,
1079 Clarke, M. F. & Newman, A. M.2020 Single-cell transcriptional diversity is a hallmark of developmental
1080 potential. *Science* **367**, 405-411, doi:367/6476/405 [pii] 10.1126/science.aax0249.

1081 50.Nystrom, E. E. L., Martinez-Abad, B., Arike, L., Birchenough, G. M. H., Nonnecke, E. B., Castillo, P. A.,
1082 Svensson, F., Bevins, C. L., Hansson, G. C. & Johansson, M. E. V.2021 An intercrypt subpopulation of
1083 goblet cells is essential for colonic mucus barrier function. *Science* **372**, doi:372/6539/eabb1590 [pii]
1084 10.1126/science.abb1590.
1085 51.Becker, W. R., Nevins, S. A., Chen, D. C., Chiu, R., Horning, A. M., Guha, T. K., Laquindanum, R., Mills,
1086 M., Chaib, H., Ladabaum, U., Longacre, T., Shen, J., Esplin, E. D., Kundaje, A., Ford, J. M., Curtis, C.,
1087 Snyder, M. P. & Greenleaf, W. J.2022 Single-cell analyses define a continuum of cell state and
1088 composition changes in the malignant transformation of polyps to colorectal cancer. *Nat Genet* **54**,
1089 985-995, doi:10.1038/s41588-022-01088-x [pii] 1088 [pii]10.1038/s41588-022-01088-x.
1090 52.Smillie, C. S., Biton, M., Ordovas-Montanes, J., Sullivan, K. M., Burgin, G., Graham, D. B., Herbst, R. H.,
1091 Rogel, N., Slyper, M., Waldman, J., Sud, M., Andrews, E., Velonias, G., Haber, A. L., Jagadeesh, K.,
1092 Vickovic, S., Yao, J., Stevens, C., Dionne, D., Nguyen, L. T., Villani, A. C., Hofree, M., Creasey, E. A., Huang,
1093 H., Rozenblatt-Rosen, O., Garber, J. J., Khalili, H., Desch, A. N., Daly, M. J., Ananthakrishnan, A. N.,
1094 Shalek, A. K., Xavier, R. J. & Regev, A.2019 Intra- and Inter-cellular Rewiring of the Human Colon during
1095 Ulcerative Colitis. *Cell* **178**, 714-730 e722, doi:S0092-8674(19)30732-9 [pii] 10.1016/j.cell.2019.06.029.
1096 53.Ito, G., Okamoto, R., Murano, T., Shimizu, H., Fujii, S., Nakata, T., Mizutani, T., Yui, S., Akiyama-Morio,
1097 J., Nemoto, Y., Okada, E., Araki, A., Ohtsuka, K., Tsuchiya, K., Nakamura, T. & Watanabe, M.2013
1098 Lineage-specific expression of bestrophin-2 and bestrophin-4 in human intestinal epithelial cells. *PLoS*
1099 *One* **8**, e79693, doi:PONE-D-13-25970 [pii] 10.1371/journal.pone.0079693.
1100 54.Parikh, K., Antanaviciute, A., Fawkner-Corbett, D., Jagielowicz, M., Aulicino, A., Lagerholm, C., Davis, S.,
1101 Kinchen, J., Chen, H. H., Alham, N. K., Ashley, N., Johnson, E., Hublitz, P., Bao, L., Lukomska, J., Andev,
1102 R. S., Bjorklund, E., Kessler, B. M., Fischer, R., Goldin, R., Koohy, H. & Simmons, A.2019 Colonic epithelial
1103 cell diversity in health and inflammatory bowel disease. *Nature* **567**, 49-55, doi:10.1038/s41586-019-
1104 0992-y [pii] 10.1038/s41586-019-0992-y.
1105 55.Peregrina, K., Houston, M., Daroqui, C., Dhima, E., Sellers, R. S. & Augenlicht, L. H.2015 Vitamin D is a
1106 determinant of mouse intestinal Lgr5 stem cell functions. *Carcinogenesis* **36**, 25-31, doi:bgu221 [pii]
1107 10.1093/carcin/bgu221.
1108 56.Tomasetti, C. & Vogelstein, B.2015 Cancer etiology. Variation in cancer risk among tissues can be
1109 explained by the number of stem cell divisions. *Science* **347**, 78-81, doi:10.1126/science.1260825.
1110 57.Wu, S., Powers, S., Zhu, W. & Hannun, Y. A.2016 Substantial contribution of extrinsic risk factors to
1111 cancer development. *Nature* **529**, 43-47, doi:10.1038/nature16166.

1112 58.Jones, J. C., Brindley, C. D., Elder, N. H., Myers, M. G., Jr., Rajala, M. W., Dekaney, C. M., McNamee, E.
1113 N., Frey, M. R., Shroyer, N. F. & Dempsey, P. J.2019 Cellular Plasticity of Defa4(Cre)-Expressing Paneth
1114 Cells in Response to Notch Activation and Intestinal Injury. *Cell Mol Gastroenterol Hepatol* **7**, 533-554,
1115 doi:S2352-345X(18)30167-X [pii] 10.1016/j.jcmgh.2018.11.004.
1116 59.Bankhead, P., Loughrey, M. B., Fernandez, J. A., Dombrowski, Y., McArt, D. G., Dunne, P. D., McQuaid,
1117 S., Gray, R. T., Murray, L. J., Coleman, H. G., James, J. A., Salto-Tellez, M. & Hamilton, P. W.2017 QuPath:
1118 Open source software for digital pathology image analysis. *Sci Rep* **7**, 16878, doi:10.1038/s41598-017-
1119 17204-5 [pii] 17204 [pii] 10.1038/s41598-017-17204-5.
1120 60.Sato, T., Vries, R. G., Snippert, H. J., van de Wetering, M., Barker, N., Stange, D. E., van Es, J. H., Abo, A.,
1121 Kujala, P., Peters, P. J. & Clevers, H.2009 Single Lgr5 stem cells build crypt-villus structures in vitro
1122 without a mesenchymal niche. *Nature* **459**, 262-265, doi:nature07935 [pii] 10.1038/nature07935.
1123 61.Zheng, G. X., Terry, J. M., Belgrader, P., Ryvkin, P., Bent, Z. W., Wilson, R., Ziraldo, S. B., Wheeler, T. D.,
1124 McDermott, G. P., Zhu, J., Gregory, M. T., Shuga, J., Montesclaros, L., Underwood, J. G., Masquelier, D.
1125 A., Nishimura, S. Y., Schnall-Levin, M., Wyatt, P. W., Hindson, C. M., Bharadwaj, R., Wong, A., Ness, K.
1126 D., Beppu, L. W., Deeg, H. J., McFarland, C., Loeb, K. R., Valente, W. J., Ericson, N. G., Stevens, E. A.,
1127 Radich, J. P., Mikkelsen, T. S., Hindson, B. J. & Bielas, J. H.2017 Massively parallel digital transcriptional
1128 profiling of single cells. *Nat Commun* **8**, 14049, doi:ncomms14049 [pii] 10.1038/ncomms14049.
1129 62.Hao, Y., Hao, S., Andersen-Nissen, E., Mauck, W. M., 3rd, Zheng, S., Butler, A., Lee, M. J., Wilk, A. J.,
1130 Darby, C., Zager, M., Hoffman, P., Stoeckius, M., Papalexi, E., Mimitou, E. P., Jain, J., Srivastava, A.,
1131 Stuart, T., Fleming, L. M., Yeung, B., Rogers, A. J., McElrath, J. M., Blish, C. A., Gottardo, R., Smibert, P.
1132 & Satija, R.2021 Integrated analysis of multimodal single-cell data. *Cell* **184**, 3573-3587 e3529,
1133 doi:S0092-8674(21)00583-3 [pii] 10.1016/j.cell.2021.04.048.
1134 63.McGinnis, C. S., Murrow, L. M. & Gartner, Z. J.2019 DoubletFinder: Doublet Detection in Single-Cell
1135 RNA Sequencing Data Using Artificial Nearest Neighbors. *Cell Syst* **8**, 329-337 e324, doi:S2405-
1136 4712(19)30073-0 [pii] 10.1016/j.cels.2019.03.003.
1137 64.Hanzelmann, S., Castelo, R. & Guinney, J.2013 GSVA: gene set variation analysis for microarray and
1138 RNA-seq data. *BMC Bioinformatics* **14**, 7, doi:1471-2105-14-7 [pii] 10.1186/1471-2105-14-7.
1139 65.Chen, Y., Chen, Y., Shi, C., Huang, Z., Zhang, Y., Li, S., Li, Y., Ye, J., Yu, C., Li, Z., Zhang, X., Wang, J., Yang,
1140 H., Fang, L. & Chen, Q.2018 SOAPnuke: a MapReduce acceleration-supported software for integrated
1141 quality control and preprocessing of high-throughput sequencing data. *Gigascience* **7**, 1-6, doi:4689118
1142 [pii] 10.1093/gigascience/gix120.

1143 66.Dobin, A., Davis, C. A., Schlesinger, F., Drenkow, J., Zaleski, C., Jha, S., Batut, P., Chaisson, M. & Gingeras,
1144 T. R.2013 STAR: ultrafast universal RNA-seq aligner. *Bioinformatics* **29**, 15-21, doi:bts635 [pii]
1145 10.1093/bioinformatics/bts635.
1146 67.Tarasov, A., Vilella, A. J., Cuppen, E., Nijman, I. J. & Prins, P.2015 Sambamba: fast processing of NGS
1147 alignment formats. *Bioinformatics* **31**, 2032-2034, doi:btv098 [pii] 10.1093/bioinformatics/btv098.
1148 68.Liao, Y., Smyth, G. K. & Shi, W.2014 featureCounts: an efficient general purpose program for assigning
1149 sequence reads to genomic features. *Bioinformatics* **30**, 923-930, doi:btt656 [pii]
1150 10.1093/bioinformatics/btt656.
1151 69.Love, M. I., Huber, W. & Anders, S.2014 Moderated estimation of fold change and dispersion for RNA-
1152 seq data with DESeq2. *Genome Biol* **15**, 550, doi:s13059-014-0550-8 [pii] 10.1186/s13059-014-0550-8.
1153 70.McKenna, A., Hanna, M., Banks, E., Sivachenko, A., Cibulskis, K., Kernytsky, A., Garimella, K., Altshuler,
1154 D., Gabriel, S., Daly, M. & DePristo, M. A.2010 The Genome Analysis Toolkit: a MapReduce framework
1155 for analyzing next-generation DNA sequencing data. *Genome Res* **20**, 1297-1303, doi:gr.107524.110
1156 [pii] 10.1101/gr.107524.110.
1157 71.Stuart, T., Srivastava, A., Madad, S., Lareau, C. A. & Satija, R.2021 Single-cell chromatin state analysis
1158 with Signac. *Nat Methods* **18**, 1333-1341, doi:10.1038/s41592-021-01282-5 [pii] 10.1038/s41592-021-
1159 01282-5.
1160 72.Haber, A. L., Biton, M., Rogel, N., Herbst, R. H., Shekhar, K., Smillie, C., Burgin, G., Delorey, T. M., Howitt,
1161 M. R., Katz, Y., Tirosh, I., Beyaz, S., Dionne, D., Zhang, M., Raychowdhury, R., Garrett, W. S., Rozenblatt-
1162 Rosen, O., Shi, H. N., Yilmaz, O., Xavier, R. J. & Regev, A.2017 A single-cell survey of the small intestinal
1163 epithelium. *Nature* **551**, 333-339, doi:nature24489 [pii] 10.1038/nature24489.
1164 73.Dann, E., Henderson, N. C., Teichmann, S. A., Morgan, M. D. & Marioni, J. C.2022 Differential
1165 abundance testing on single-cell data using k-nearest neighbor graphs. *Nat Biotechnol* **40**, 245-253,
1166 doi:10.1038/s41587-021-01033-z [pii] 10.1038/s41587-021-01033-z.

1167

Acknowledgements

We thank E. Bindels and R. Hoogenboezem for their support to generate the single cell sequencing data, J.D. Windster for help with in situ hybridizations, W.S. van de Geer for analysis support of bulk sequencing data; W. Szymanska, E. Middendorp Guerra and E. de Vet for help with the IHC and scRNAseq analyses; V.H.A.E. Verhagen for discussions on XGBoost machine learning. This study was financially supported by the Dutch Cancer Society (KWF; project no. 11407), the Wereld Kanker Onderzoek Fonds and World Cancer Research Funds (WKOF/WCRF; projects no. 2014-1181 and IIG_FULL_2022_015), and in part by the National Cancer Institute (NCI; project no. R01CA214625, R01CA229216, and P30-013330), the National Institute on Aging (NIA; project no. P30 AG038072, 5T32AG023475-20), Academy of Finland (Finnish Center of Excellence Program 2018–2025 312041, Academy Professor grant no. 319083 and 320149), iCAN Digital Precision Cancer Medicine Flagship (320185), Cancer Society of Finland, Sigrid Jusélius Foundation (220002), and the Jane and Aatos Erkko Foundation.

Author contributions

M.P.V., R.J., M.S. and A.S. designed and performed experiments. M.P.V., J.C., N.V., L.A.A. and L.H.A. generated and analyzed sequencing data sets. K.R., P.P, S.S, B.v.d.S. and T.P.P.v.d.B. performed immunohistochemistry. D.S. and M.D. were responsible for pathological examination and IBD patient selection. M.P.V. and R.F. wrote the manuscript. R.F. supervised the study and was responsible for concept and design of the study.

Competing interests

The authors declare no competing interests.

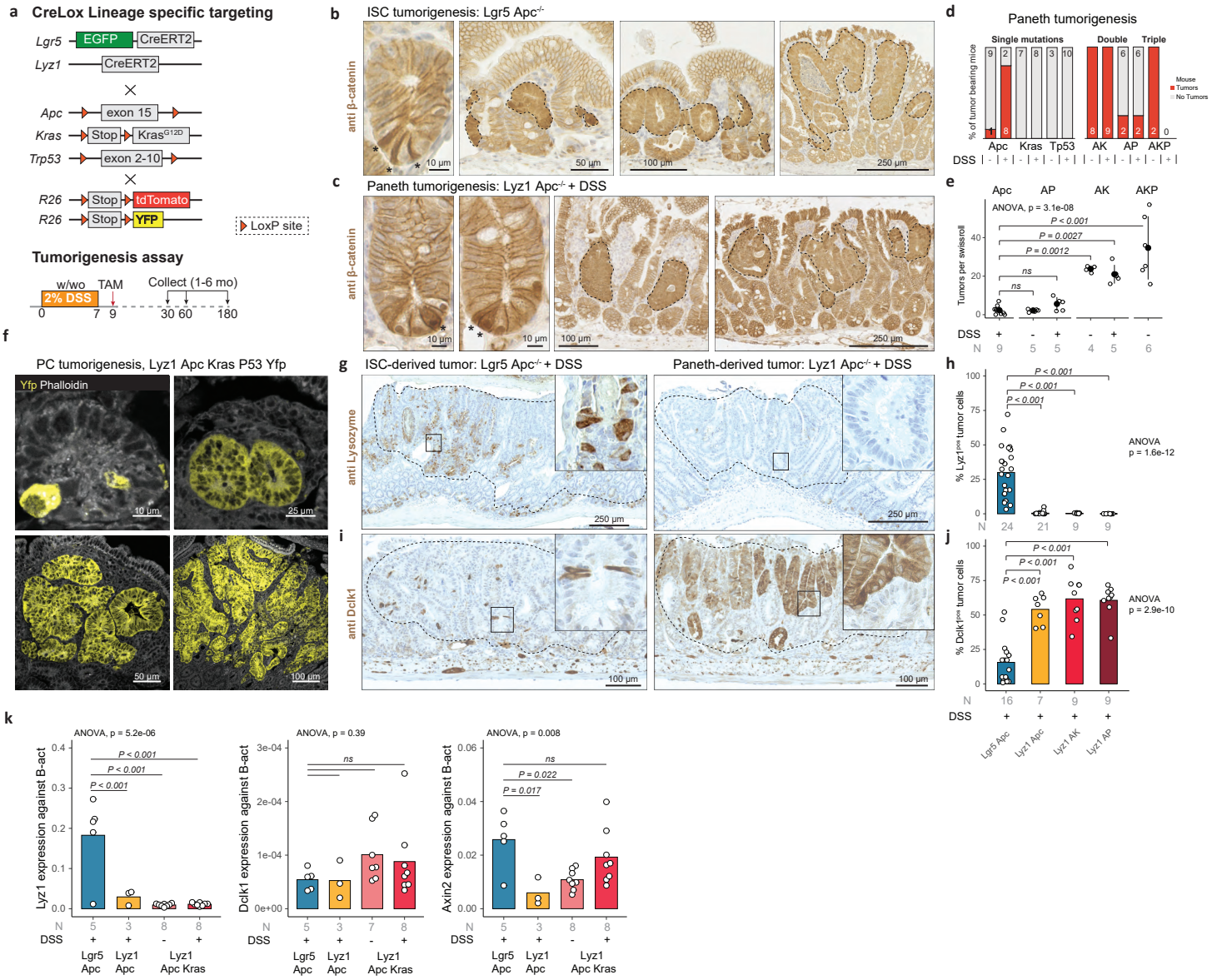

Fig. 1 | Paneth cells as the cell-of-origin of intestinal cancer.

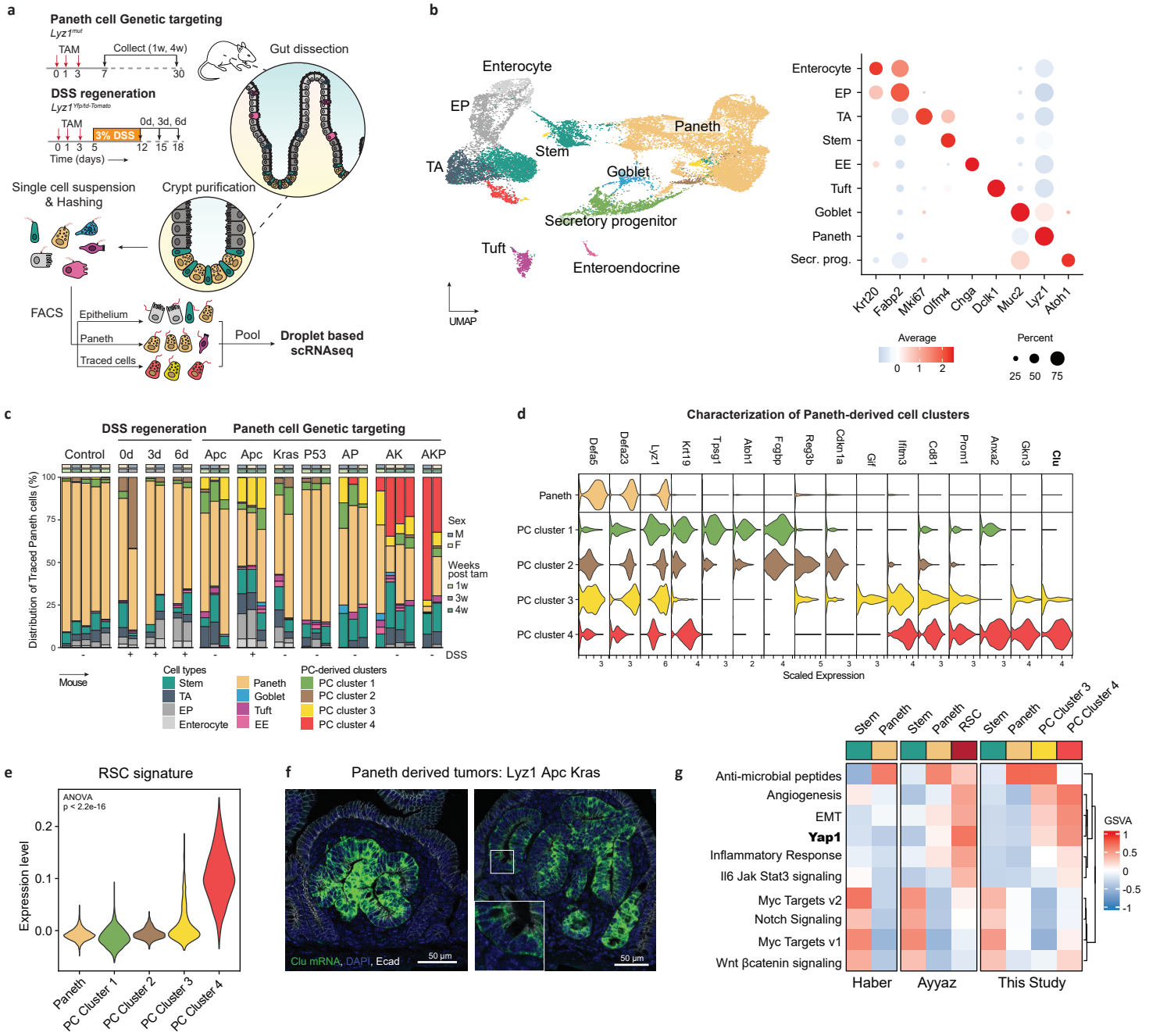

Fig. 2 | Paneth cells dedifferentiate into a revival stem cell identity.

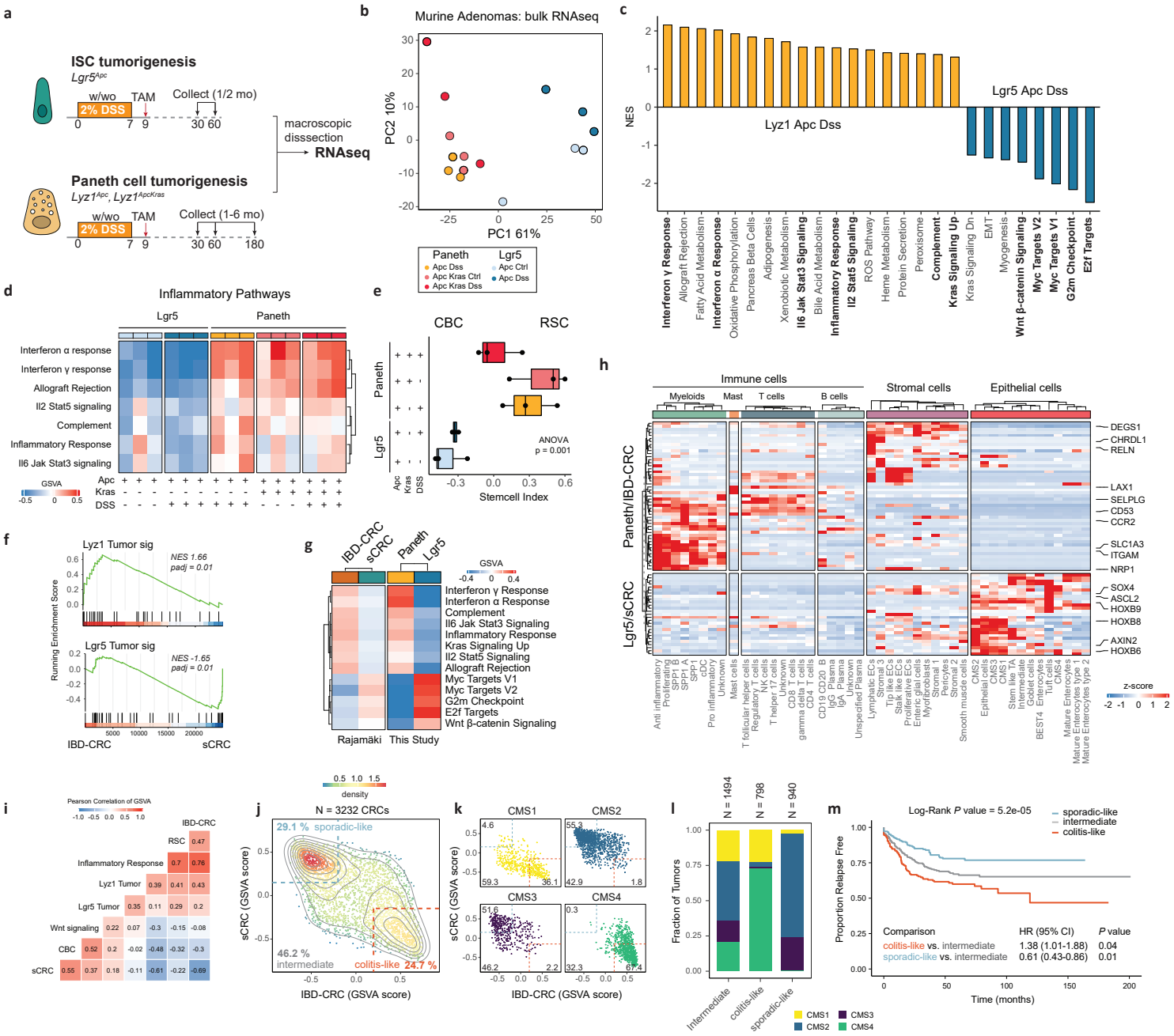

Fig. 3 | Paneth-derived adenomas have an inflammatory phenotype mimicking colitis-associated cancer.

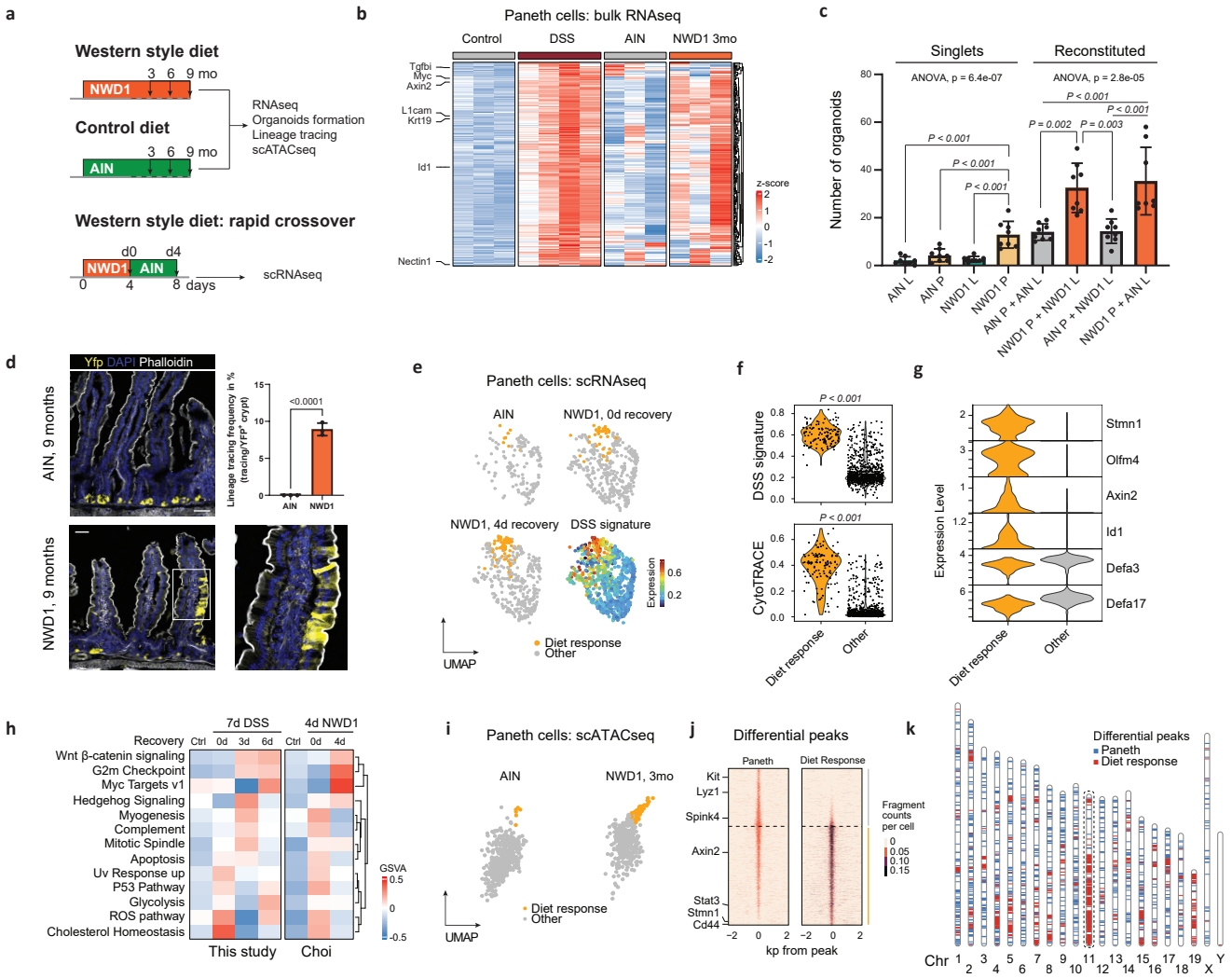

Fig. 4 | Western-style diet triggers an inflammatory response leading to dedifferentiation of Paneth cells.

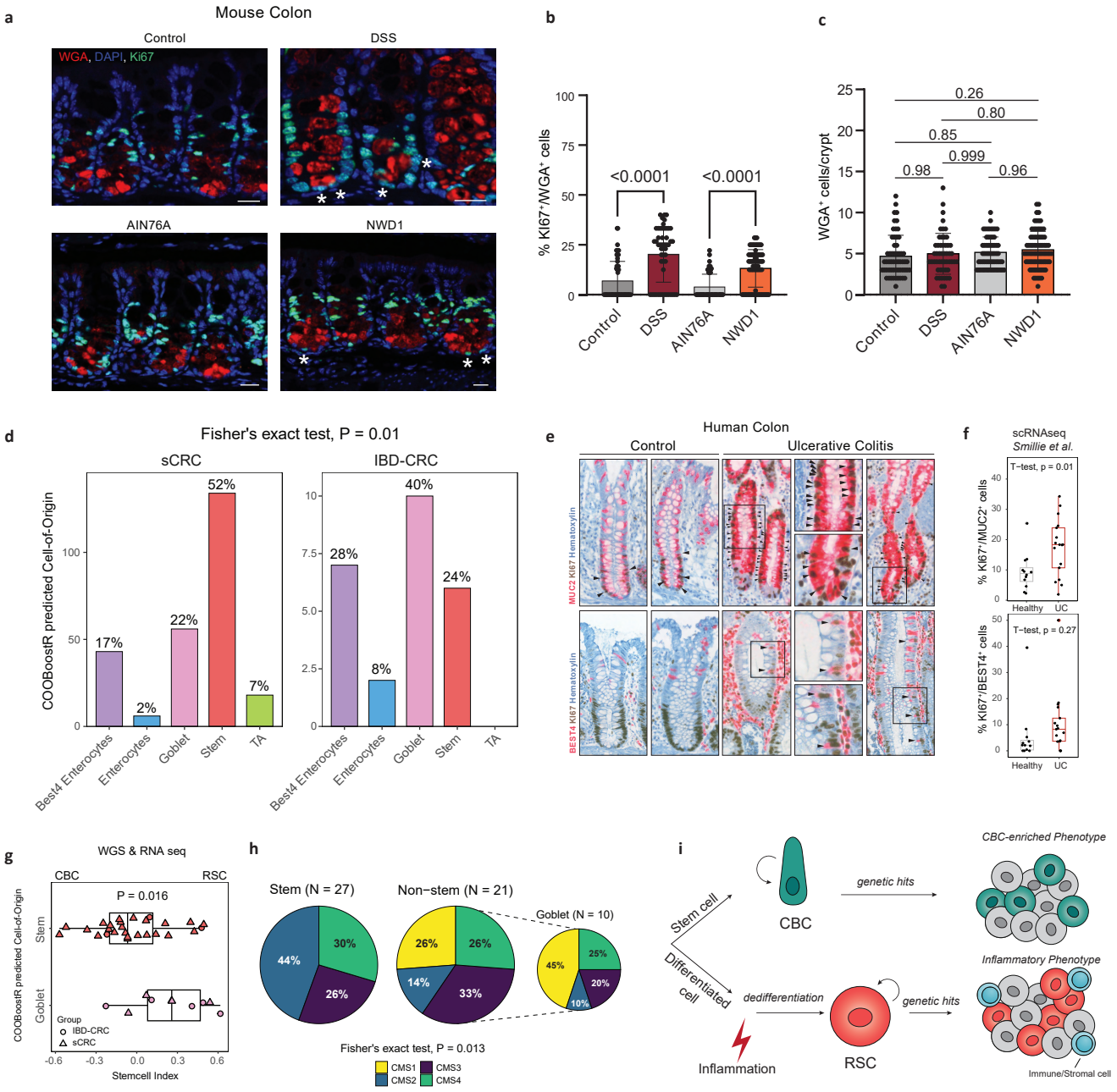

Fig. 5 | Inflammation activates distinct cells of origin in the colon.

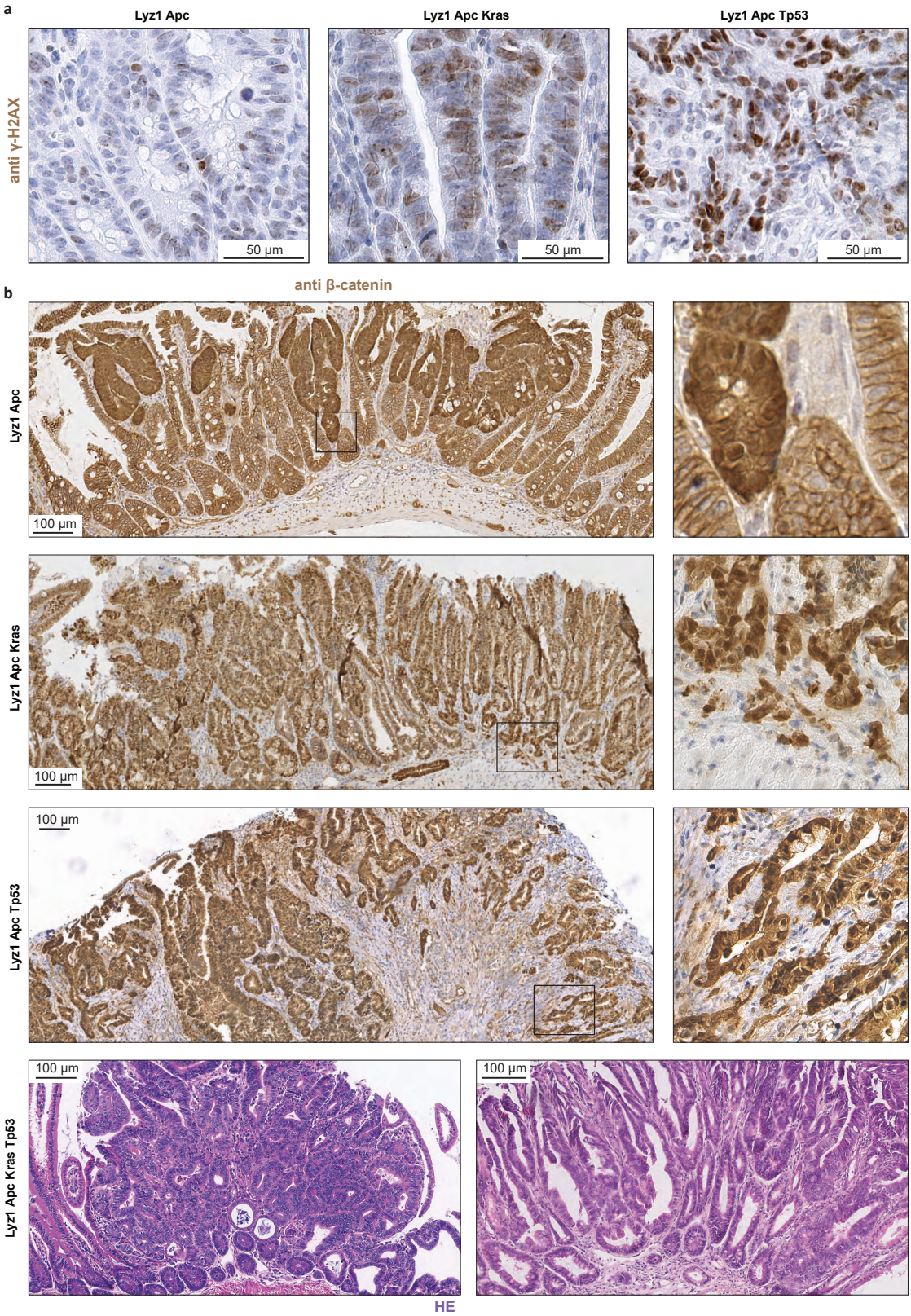

Suppl. Fig. 1 | Immuno-histologic analysis of Paneth-derived tumors.

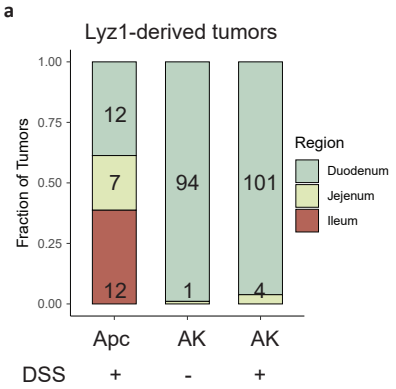

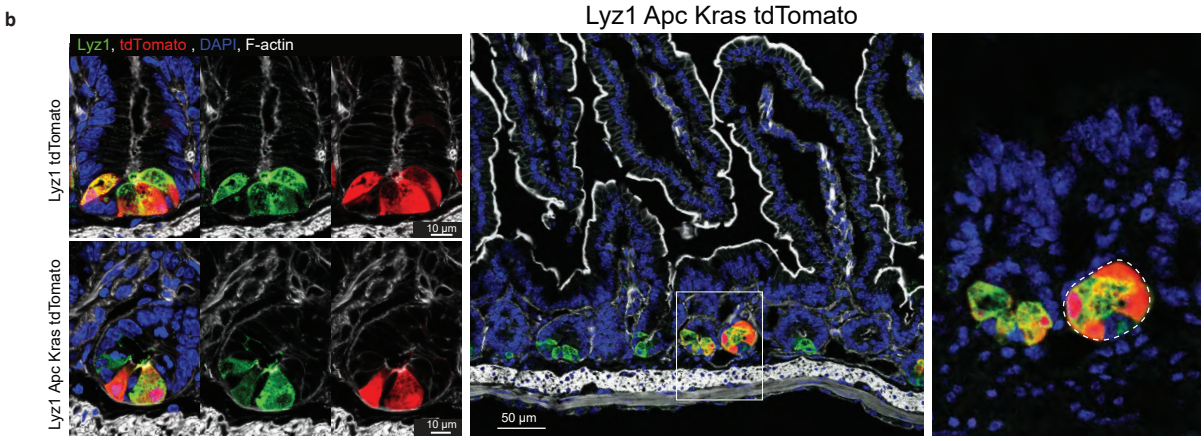

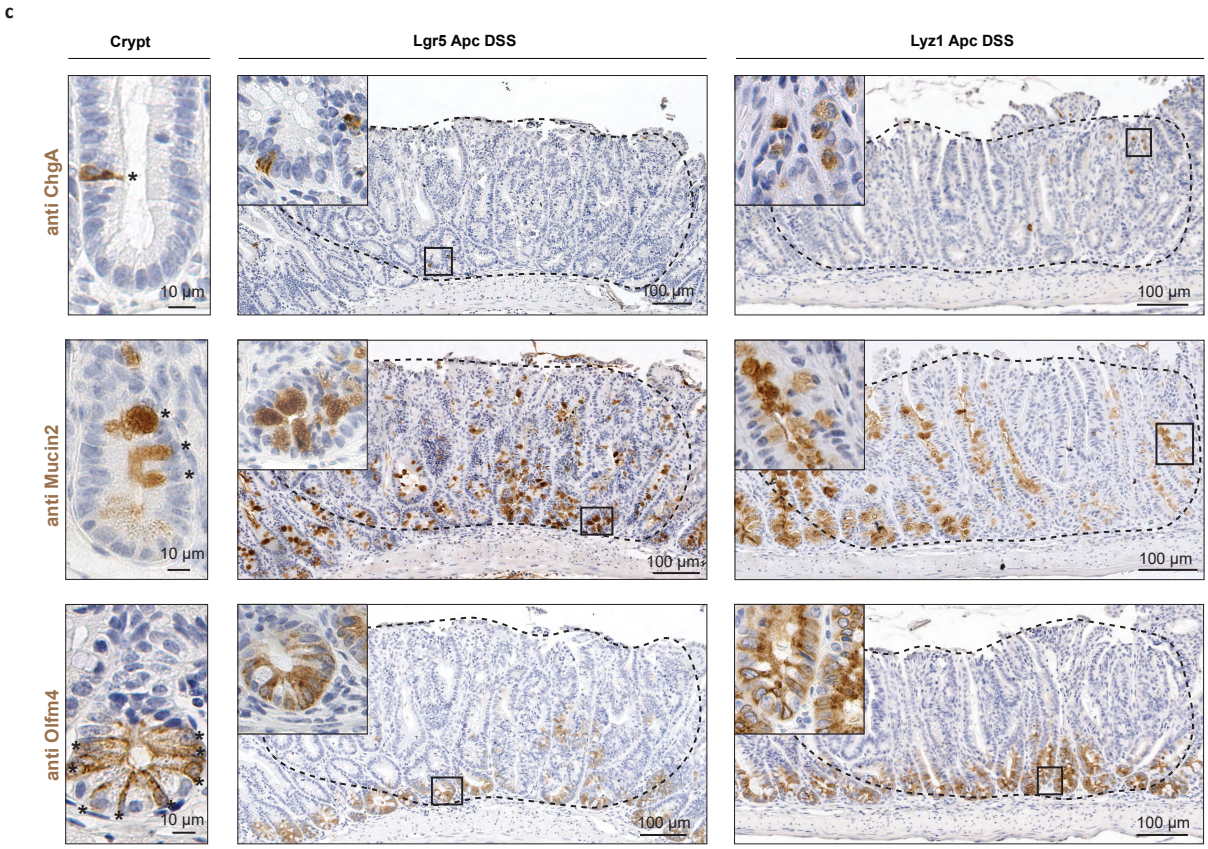

Suppl. Fig. 2 | Characterization of PC-derived small intestinal adenomas.

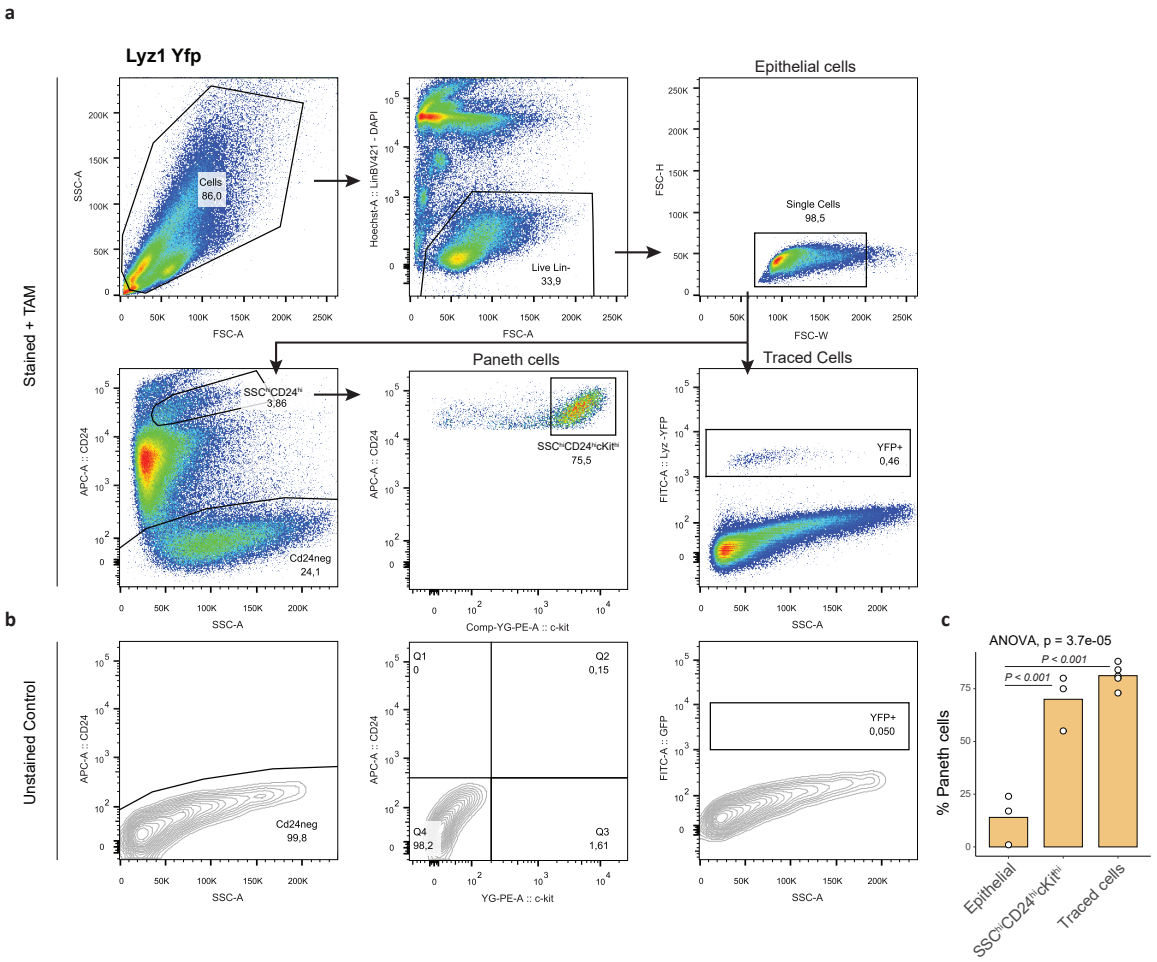

Suppl. Fig. 3 | FACS gating strategy for Paneth cells enrichment and isolation.

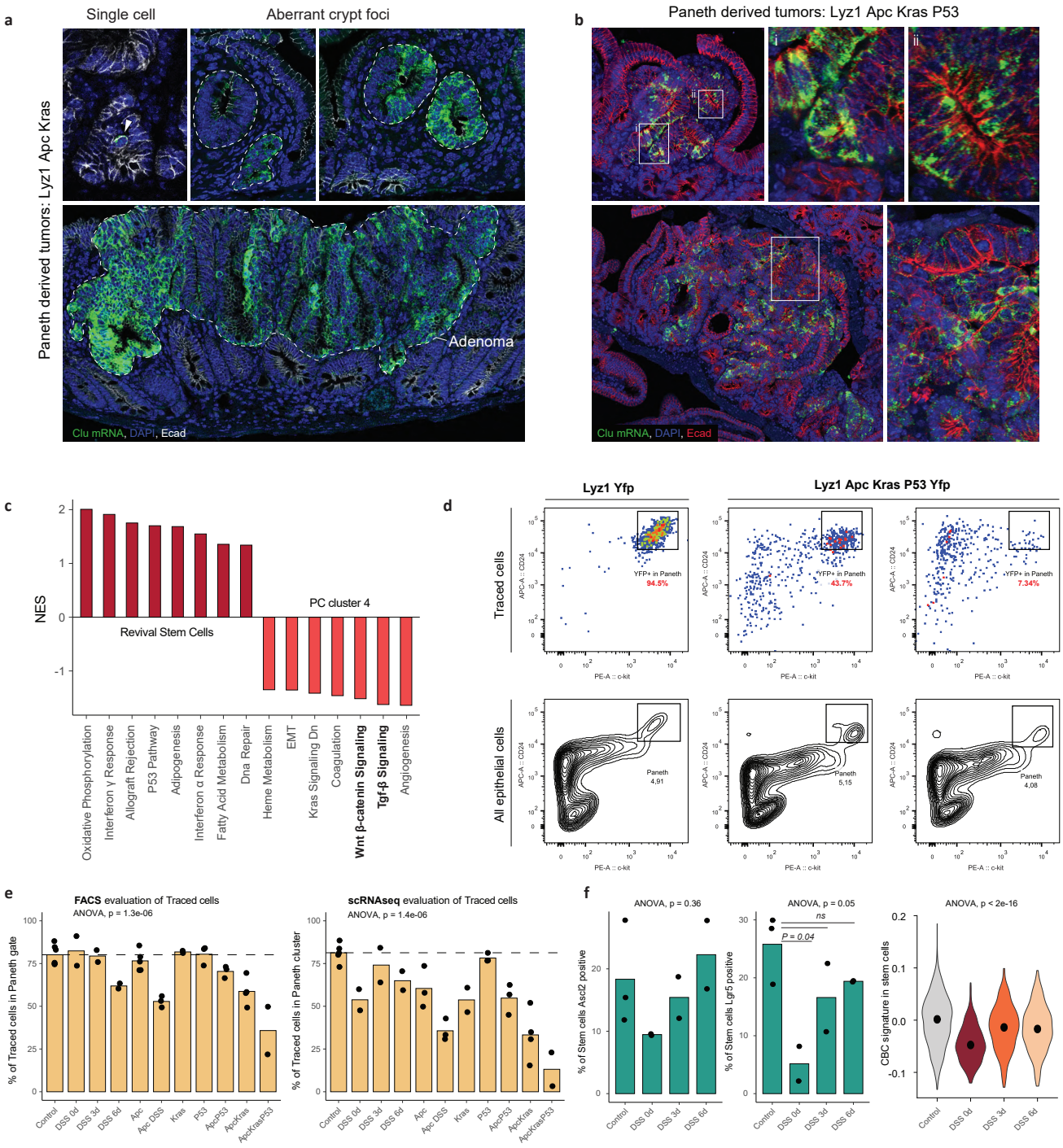

Suppl. Fig. 4 | Paneth cells dedifferentiate upon DSS-driven inflammation and genetic targeting.

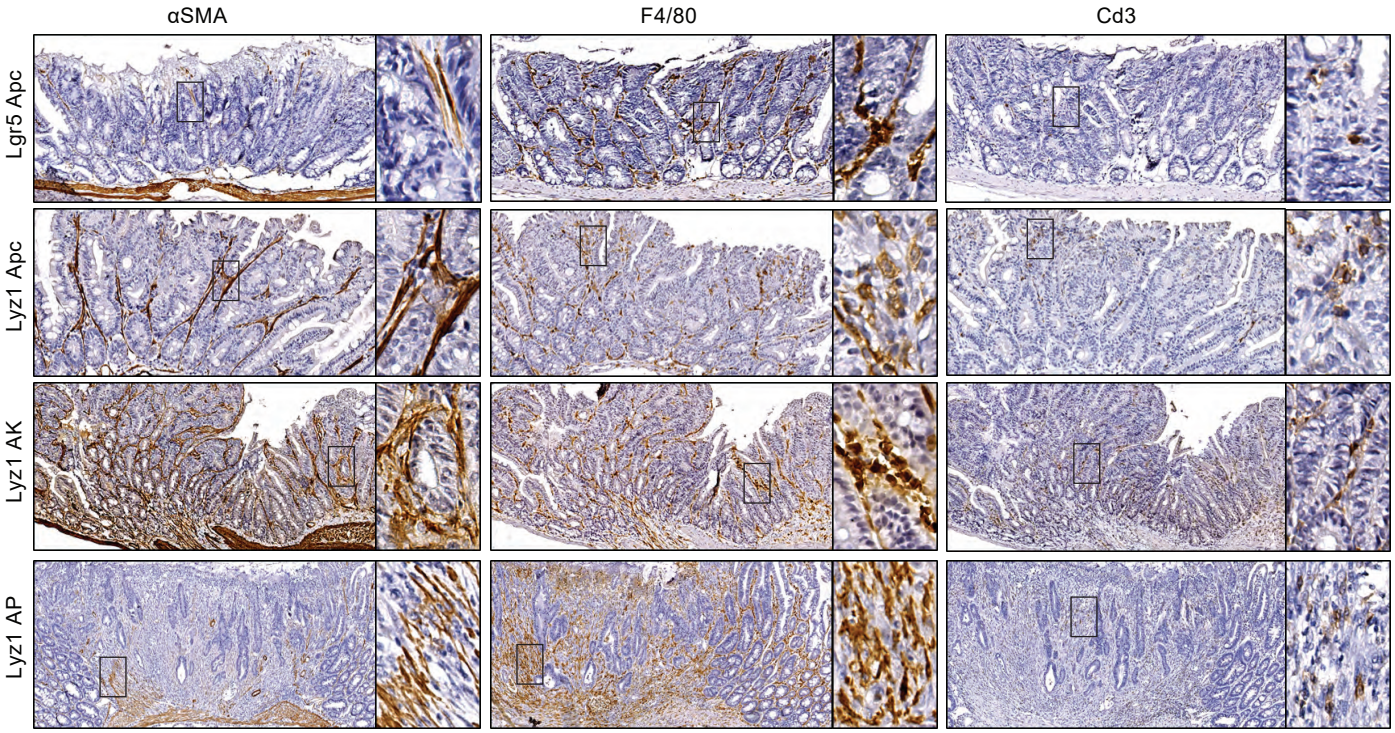

Suppl. Fig. 5 | Distinct TME features in CBC- and PC-derived small intestinal adenomas.

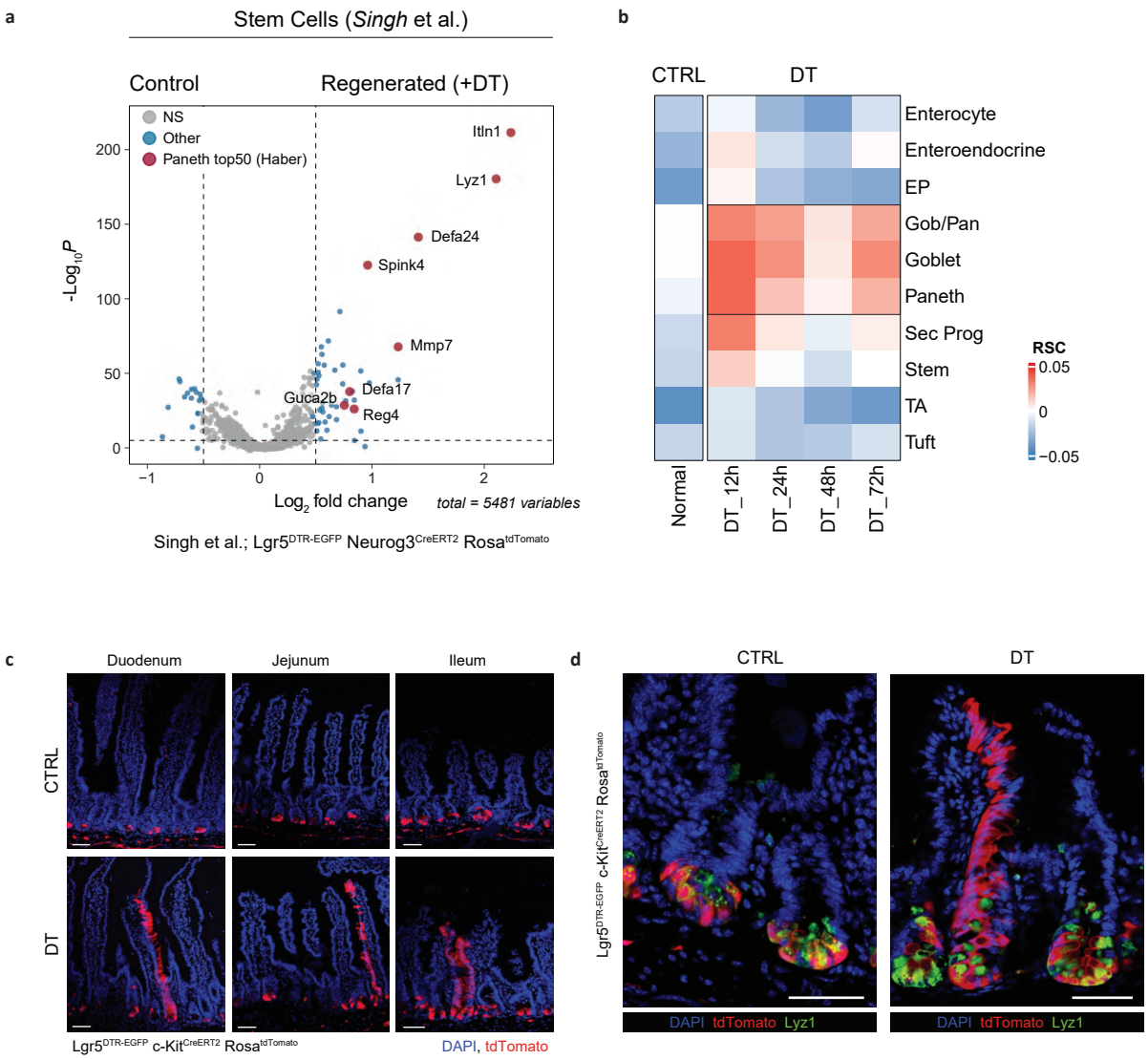

Suppl. Fig. 6 | Lgr5⁺ CBCs ablation triggers dedifferentiation of Paneth and goblet secretory lineages.

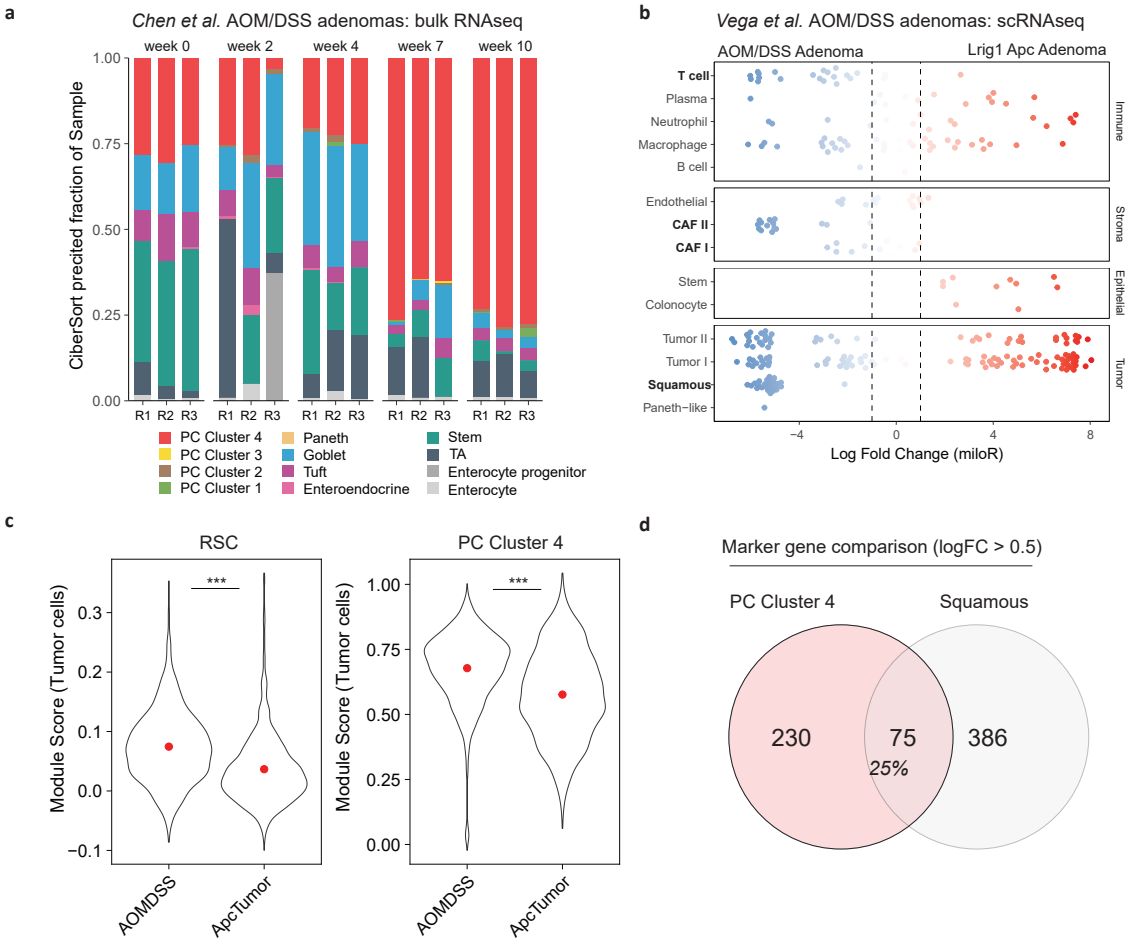

Suppl. Fig. 7 | AOM/DSS-derived adenomas share similarities with PC-derived tumors.

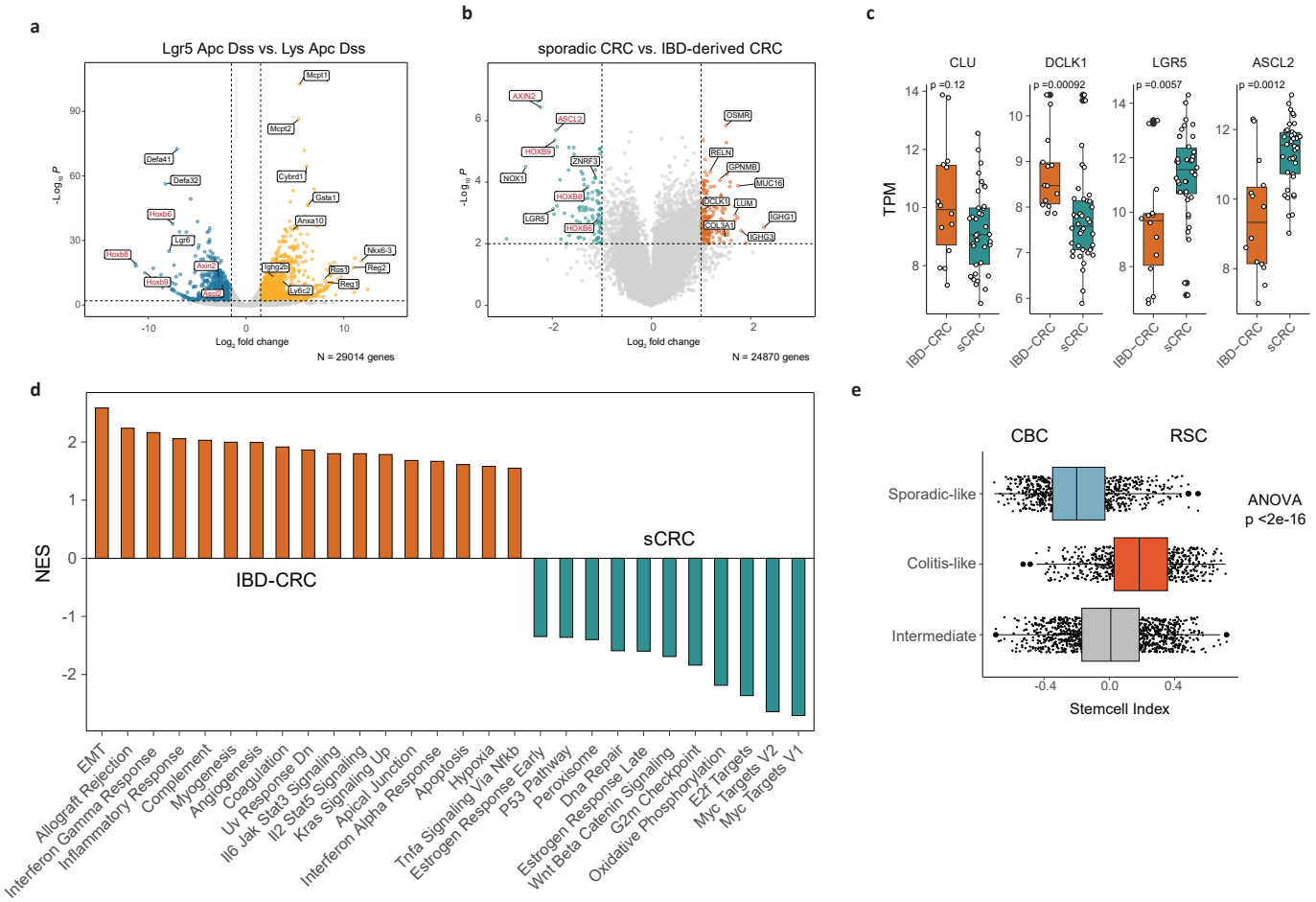

Suppl. Fig. 8 | Differential gene expression comparative analysis between IBD colon cancers and murine PC-derived small intestinal adenomas.

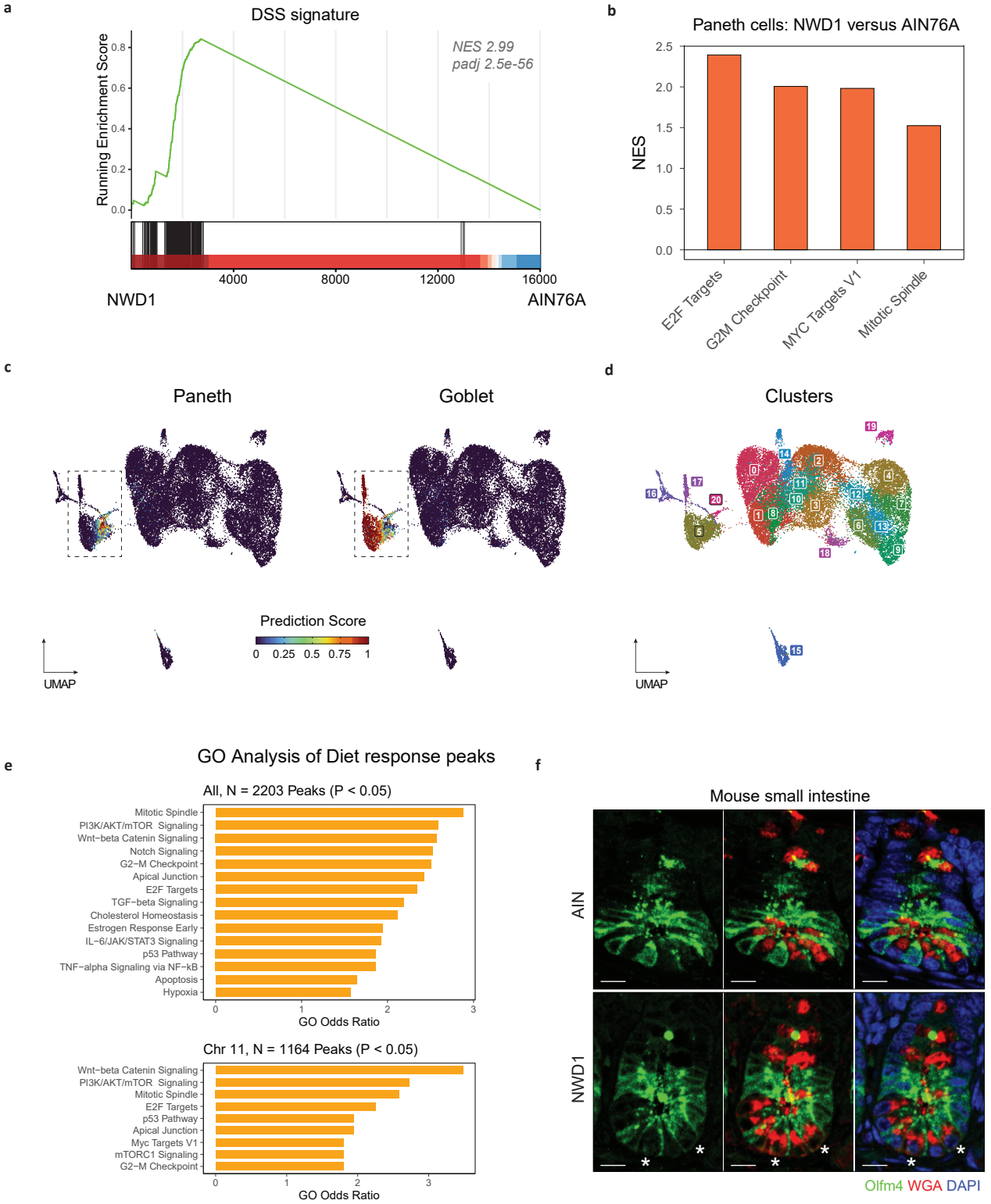

Suppl. Fig. 9 | The NWD1 western-style diet triggers the dedifferentiation of Paneth cells.

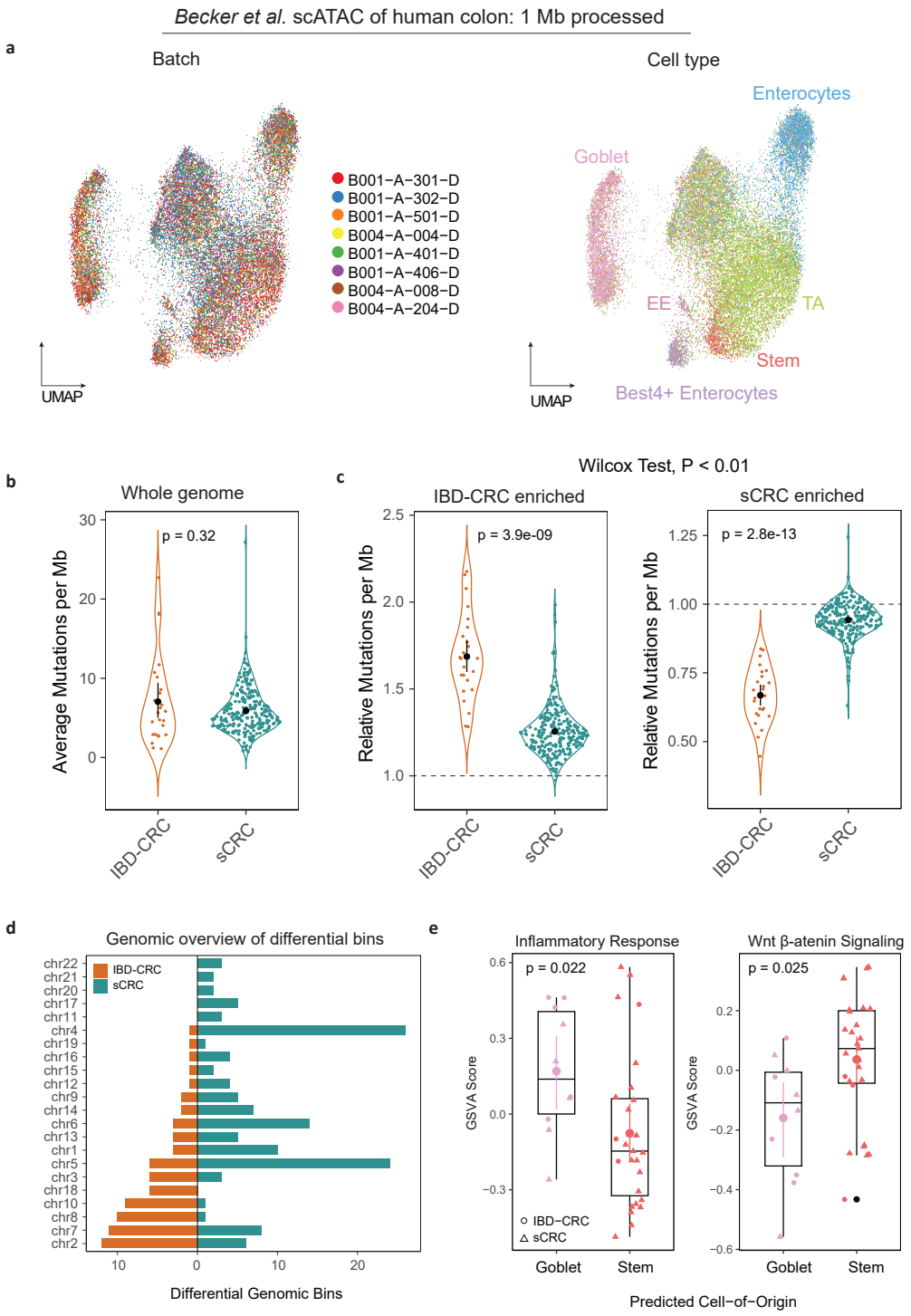

Suppl. Fig. 10 | Epigenetic profiles of normal colonic lineages and mutational patterns of IBD-related and sporadic colon cancers.